

# Testbeam Studies

## Contents

<b>1</b>	<b>Intro</b>	<b>1</b>
<b>2</b>	<b>Beamline geometry</b>	<b>2</b>
2.1	The view from above . . . . .	2
2.2	The wirechamber coordinates . . . . .	3
2.3	The rotation of the magnet . . . . .	4
<b>3</b>	<b>Wire chamber tracking - the algorithm</b>	<b>8</b>
3.1	Draw straight lines through every possible hit combination . . . . .	8
3.2	Find the track with the minimum residual . . . . .	8
3.3	Approximate the momentum based on the track's entry and exit directions from the magnetic field . . . . .	9
3.4	Correct the approximated momentum for magnetic field variations . . . . .	10
3.5	Calculating the intersections between the magnet front face and the upstream track . . . . .	10
<b>4</b>	<b>Validation of the new implementation of WCTrackAlg</b>	<b>11</b>
4.1	Counting tracks of each type . . . . .	13
4.2	Comparing track properties . . . . .	14
<b>5</b>	<b>Considerations for analysers</b>	<b>15</b>
<b>6</b>	<b>Particle types</b>	<b>33</b>
6.1	Particle speeds . . . . .	34
<b>7</b>	<b>Detector</b>	<b>37</b>
7.1	The baby NOvA coordinates . . . . .	37
7.2	Structure: Cells and Planes . . . . .	37
7.3	Hit properties . . . . .	42
7.4	Kinetic energy versus last plane with hit . . . . .	42
<b>8</b>	<b>All the plots: detector plane rotations</b>	<b>42</b>
<b>9</b>	<b>All the plots: Energy versus x/y</b>	<b>42</b>

## 1 Intro

This tech note is under heavy development!

Documentation of the plots and notes made in 2023 as part of an effort to understand the testbeam data.

The WCTrackAlg is at [WCTrackAlg.cxx](#).

There are four wire chambers in the NOvA testbeam beamline setup, with two on either side of the magnet. The thinking is that a particle from the tertiary beam will traverse all four wire chambers on its way to the baby NOvA detector , allowing for reconstruction of a track with a well-measured momentum and direction. This wirechamber track can be combined with the time-of-flight measurement to get a wirechamber mass, and thus a particle ID.

In practice we observe that there are quite often only 3 (or fewer) wire chambers with a signal, so it may be helpful to update the algorithm to allow for 3-point tracks.

The purpose of the study detailed in this section is to validate the changes made to the WCTrackAlg, while understanding the implications of using 3 point tracks.

The track algorithm itself is quite simple, but the geometries require a bit of thought, so the first section here is devoted to clarifying that.

After completing the new implementation of WCTrackAlg I started to look at the detector, and so this monstrous tech note continues to grow.

## 2 Beamlne geometry

### 2.1 The view from above

If one were hovering above the beamline instrumentation with their head in the direction of the beam direction, then the forward direction is positive  $z$ , to the left is positive  $x$ , and the positive  $y$  direction is upwards toward the sky. See diagram in Figure 1. The coordinates of some main components are given in Figure 2. Figure 3 shows an example trajectory of a particle through the beamline components.

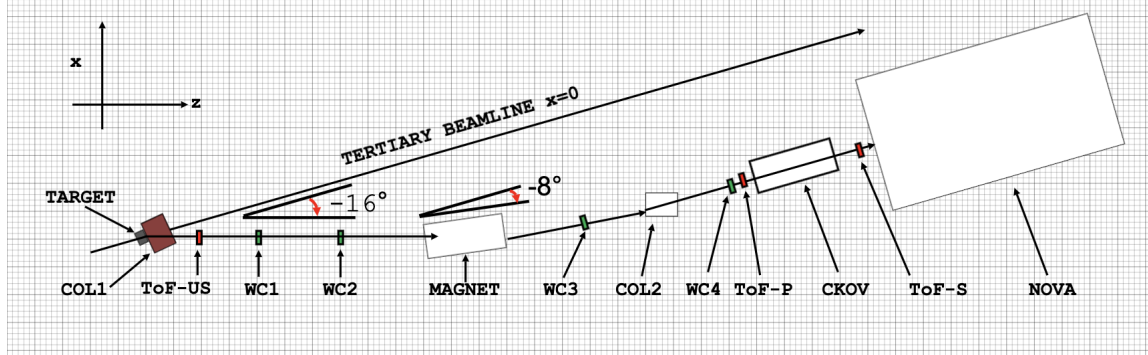


Figure 1: A sketch of the beamline instrumentation as viewed from above.

	$x$ [cm]	$y$ [cm]	$z$ [cm]	$\theta$ [degrees]
Target	0.04	-0.36	0	0
ToF US Period3&4 (2)	-40.58 (-38.55)	-0.13 (0.75)	141.57 (137.56)	-16
WC1	-45.58	0.05	159.10	-16
WC2	-86.00	0.09	299.89	-16
Magnet Center	-129.77	-0.03	472.81	-8
WC3	-135.29	0.01	736.95	0
DS Collimator	-135.96	-0.34	939.80	0
WC4	-135.39	0.03	1014.33	0
Cherenkov front	-135.35	0.05	1177.51	0
Cherenkov back	-135.36	0.11	1386.34	0
ToF DS PMT	-135.78	0.33	1441.53	0
ToF DS SiPM	-135.34	-0.05	1455.35	0
NOvA Front Face Center	-137.40	7.93	1462.16	0.04

Figure 2: Coordinates of some of the main components of the beamline instrumentation.

```
Particle trajectory: [cm] wrt origin, * wrt wc / magnet / NOvA
      Origin   hit1    *   hit2    *   Mag    *   hit3    *   hit4    *   NOvA    *
      X       1.0    -43.7   1.8   -83.3   2.7  -132.1   5.1  -132.5   2.8  -134.1   1.3  -136.7   0.7
      Y     -1.1    -1.4   -1.5   -1.4   -1.5   -1.0   -0.9   -2.1   -2.1   -2.7   -2.7   -3.6  -11.5
      Z      0.0    159.6   0.5  300.7   0.8   474.6   0.7   736.9   -0.0  1014.3   0.0  1462.2   0.0
```

Figure 3: An example trajectory of measurements along the beamline.

## 2.2 The wirechamber coordinates

Figure 5 show the hit positions in the four wirechambers. The missing wires in WC1 increase over the periods of data taking, shown in Figure 6.

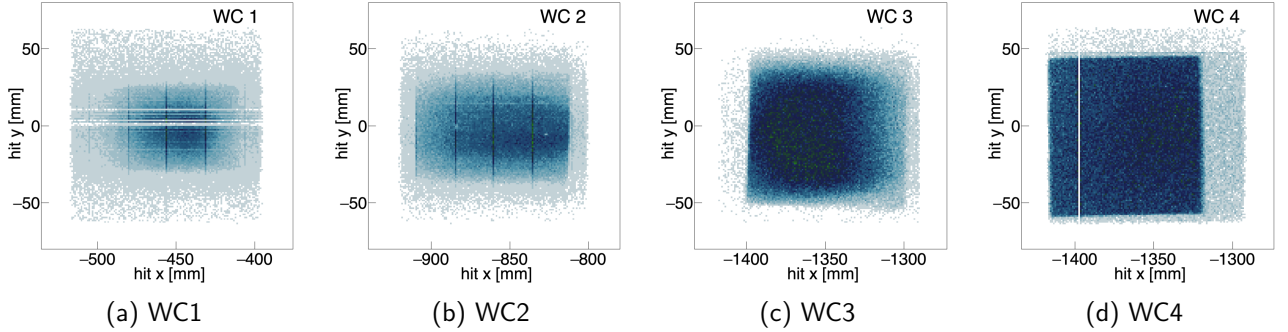


Figure 4: The WCTrack best hit position in each of the four wire chambers, relative to the collimated tertiary beam. The best hit here means the hit that was attributed to the best track fit. Notice that wire chamber 1 has missing wires. All four hits must be present for these plots to be filled

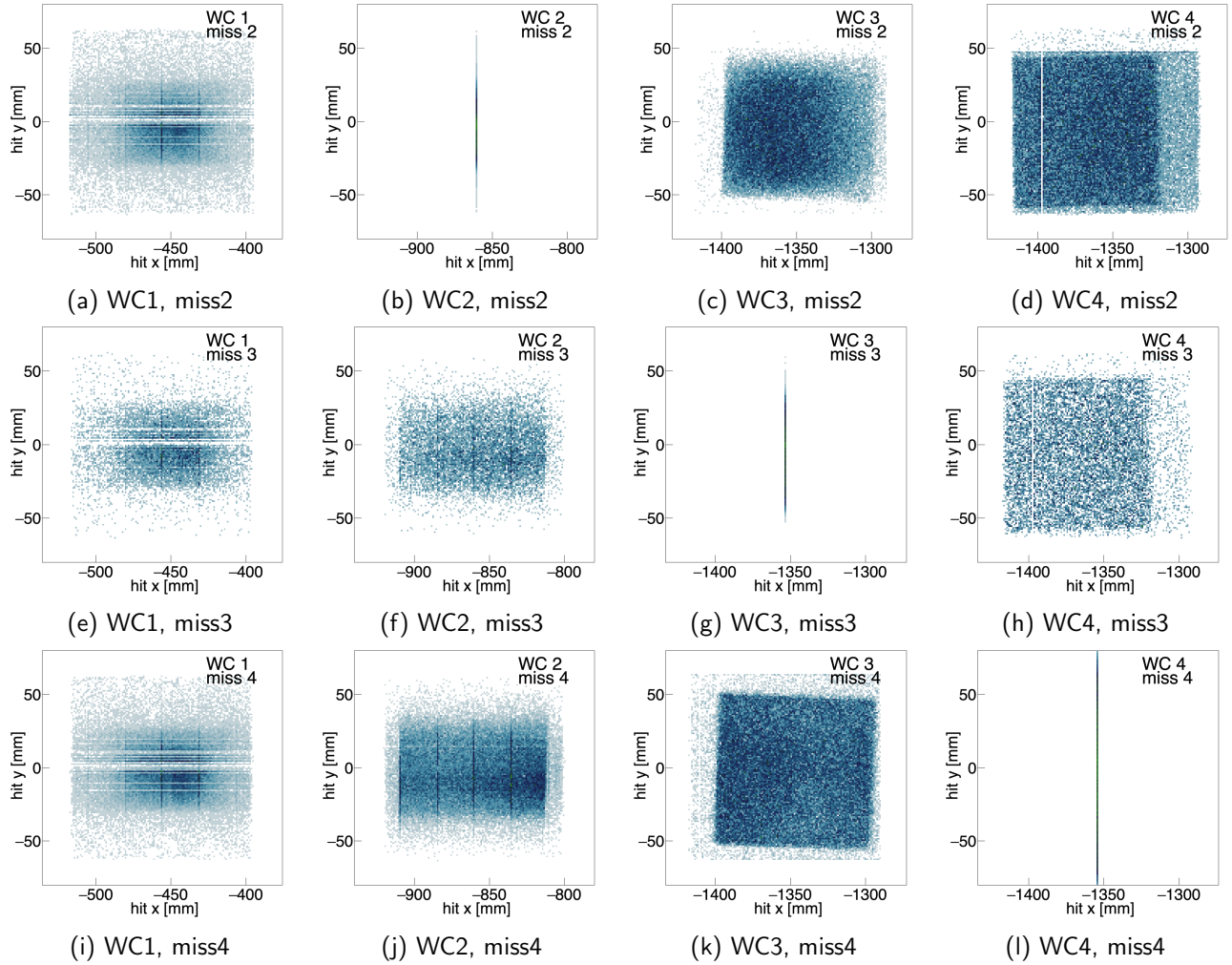


Figure 5: The WCTrack best hit position in each of the four wire chambers, relative to the collimated tertiary beam. The best hit here means the hit that was attributed to the best track fit. Notice that wire chamber 1 has missing wires. Top row: tracks where the hit in wc2 is faked, middle row: hit 2 is faked, bottom row: hit 4 is faked.

### 2.3 The rotation of the magnet

Figure 8 shows a sketch of a track passing through the magnetic field. The magnet is rotated about its center, contrary to what is shown in the technical drawings Figures 9 and 10. Figure 11 show the entry point in x,y in the magnet's frame of the upstream track.

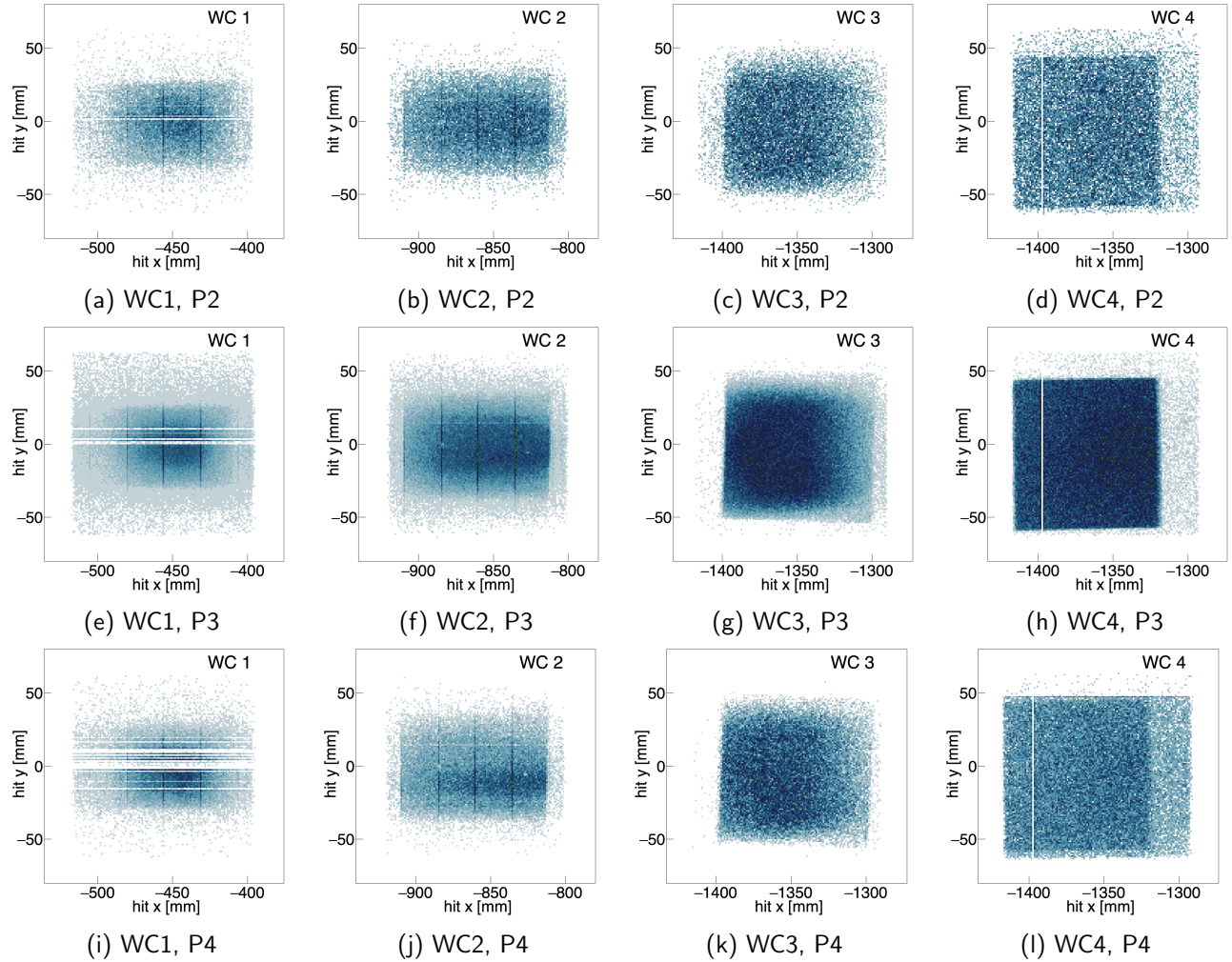


Figure 6: The WCTrack best hit position in each of the four wire chambers, divided by period.

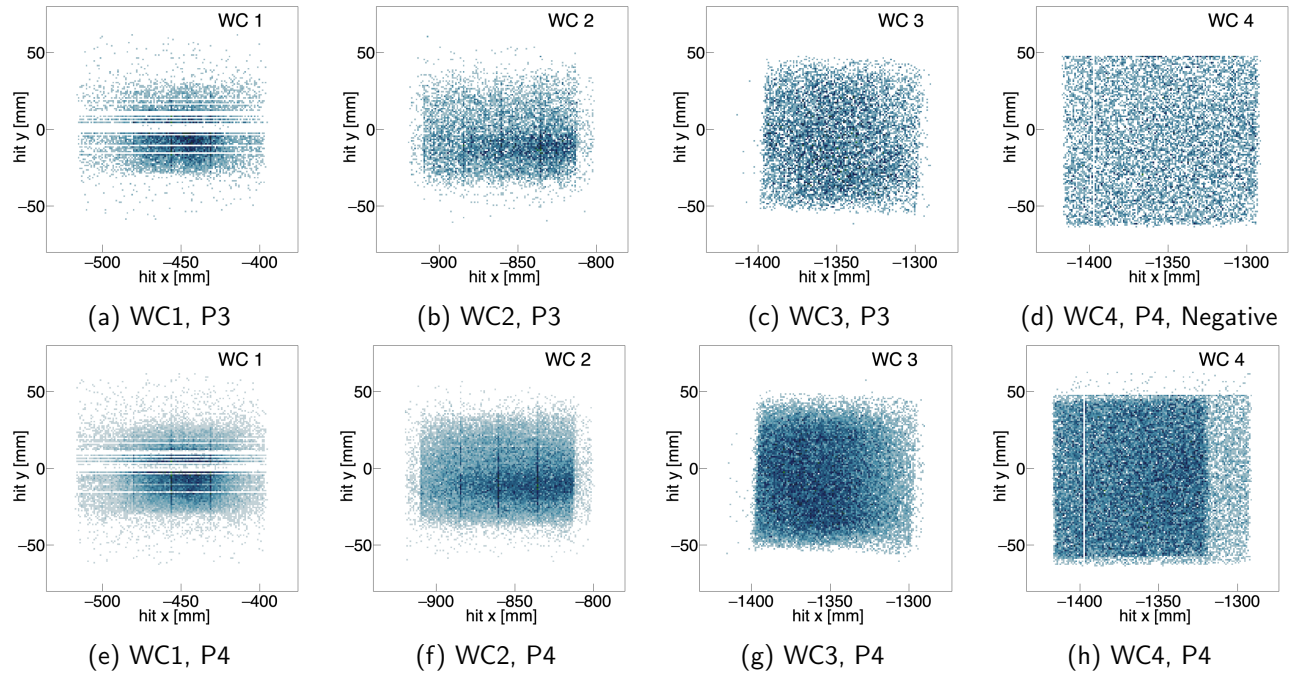


Figure 7: The WCTrack best hit position in each of the four wire chambers, in period 4, divided by polarity.

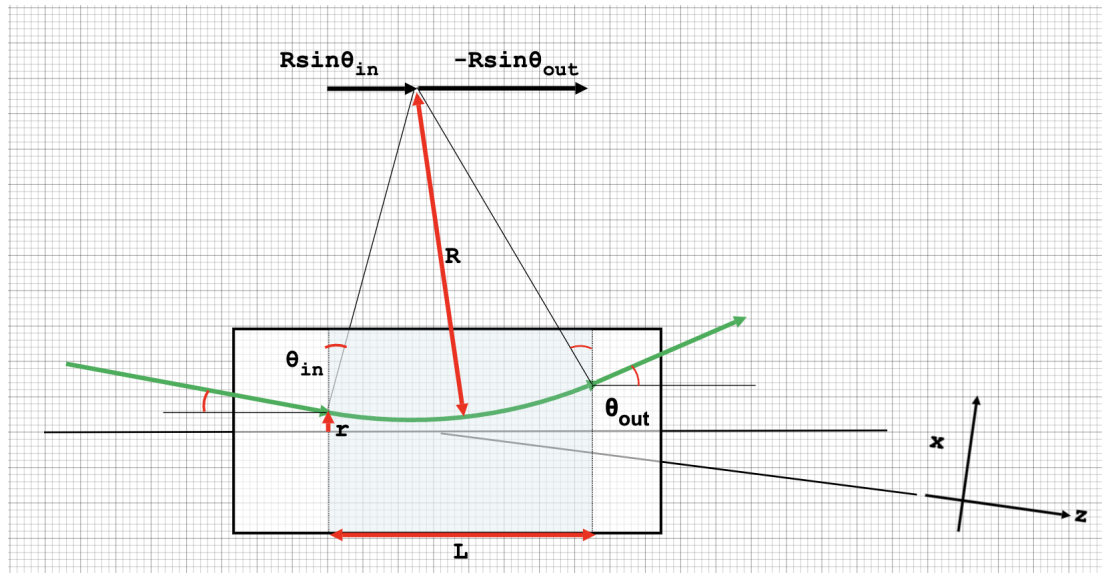


Figure 8: Magnet details.

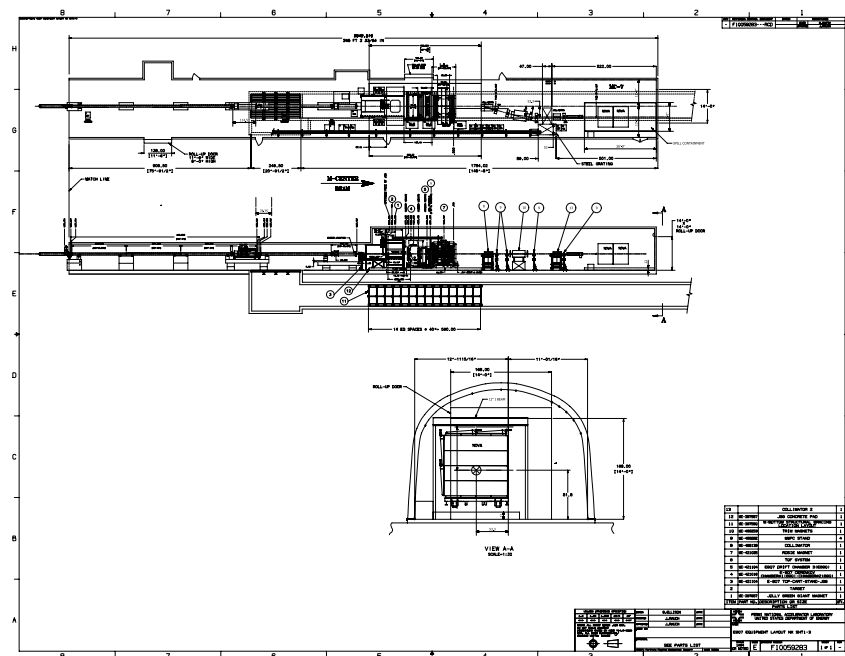


Figure 9: Technical drawing made before the decision to rotate the magnet around its center rather than its front face center.

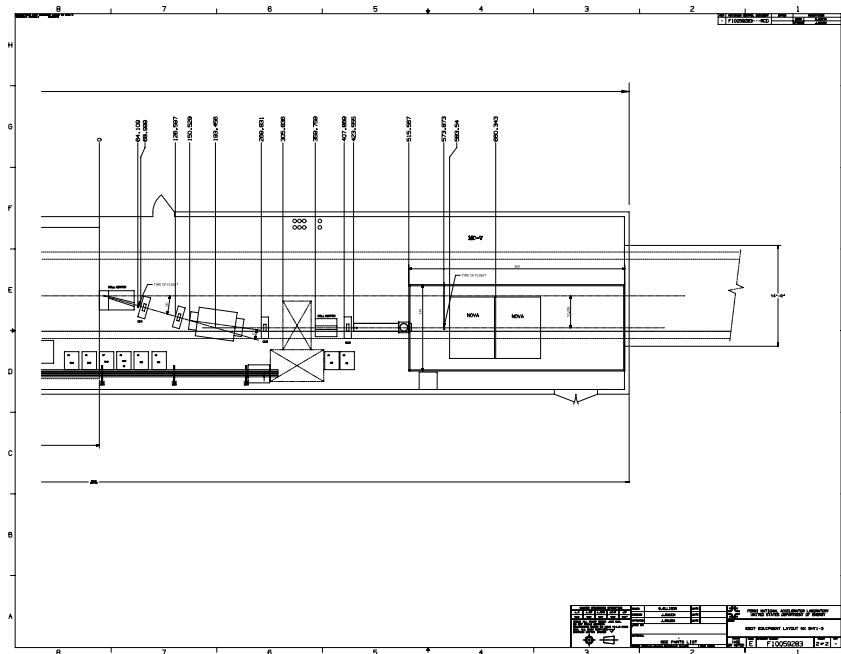


Figure 10: Technical drawing made before the decision to rotate the magnet around its center rather than its front face center.

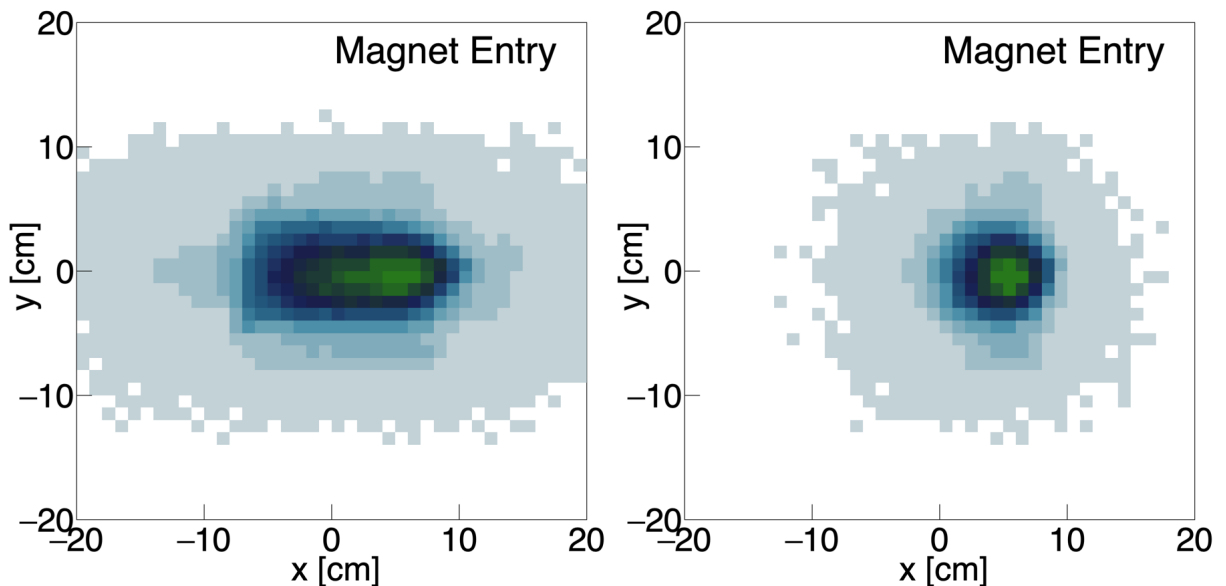


Figure 11: The x,y entry point of the upstream track to the magnetic field. On the left there is no constraint on the track having momentum consistent with the magnet current. On the right the track momentum must be within 10% of the magnet current.

### 3 Wire chamber tracking - the algorithm

The track algorithm can be roughly broken down into four parts:

1. Draw straight line tracks through every possible hit combination
2. Find the track with the minimum residual
3. Approximate the momentum based on the track's entry and exit directions from the magnetic field
4. Correct the approximated momentum for magnetic field variations

#### 3.1 Draw straight lines through every possible hit combination

Wirechamber hits are defined using the WCHitFinder which has not yet been explored as part of these studies. Each wire chamber has horizontal wires providing a y-position, and vertical wires providing an x-position. A wirechamber hit is formed from an (x,y) combination. There must be a signal on at least one vertical and at least one horizontal wire within a chamber to form a hit. If there are eg two vertical wire signals and one horizontal wire signal, then there are two hits, and so on such that  $n_{hit} = n_x \times n_y$  for any given wire chamber.

Hit positions (x,y) with respect to the centres of their wire chambers are returned by the createHits method. The WCTrackAlg then converts these into global positions, adding in the global z-coordinate of the corresponding wire chamber, and passes every combination of four hits to a simple linear regression function.

If wirechamber  $N$  does not have a hit, the algorithm can proceed providing that the other three wire chambers do have hits. In this case the missing wire chamber is ignored.

#### 3.2 Find the track with the minimum residual

For every possible combination of 3 of 4 WC hits, the straight line in the y,z plane through them is found by minimising the residuals in the least squares fit.

$$y_i = a + bz_i + e_i, \quad (1)$$

where  $a$  and  $b$  are the unknown slope and intercept parameters belonging to the best fit, which is found by minimising the residual  $e_i$ . The residual here is the distance in  $y$  between the best fit line and hit  $i$ . The slope is then:

$$b = \frac{n \sum_i z_i y_i - \sum_i z_i \sum_i y_i}{n \sum_i z_i^2 - (\sum_i z_i)^2}, \quad (2)$$

where  $n$  is the number of points (being three or four in this case) and the sum is over the hits  $i$ . The intercept is:

$$a = \frac{\sum_i y_i - b \sum_i z_i}{n}, \quad (3)$$

and the residual for point  $i$  is

$$e_i = y_i - bz_i - a. \quad (4)$$

We require that each of the three or four residuals must be within the dimensions of the wirechamber, which is roughly 12 cm from the centre. The track's goodness of fit is then based on the average of the square root of the sum of the squared residuals:

$$e_{avg} = \frac{\sqrt{\sum_i e_i^2}}{n} \quad (5)$$

with the track having the minimum average residual  $e_{avg}$  chosen.

### 3.3 Approximate the momentum based on the track's entry and exit directions from the magnetic field

A charged particle with transverse momentum  $p_T$  entering a magnetic field of strength  $B$  will follow a curved path with radius  $R$  according to:

$$p_T = qBR, \quad (6)$$

where  $q$  is the charge and the units are  $\text{kg m s}^{-1}$ . The following procedure is used to convert the units of momentum to the preferred  $\text{GeV}/c$ :

$$\begin{aligned} p_{TC} &= qBRc \text{ [Joules]} \\ &= qBRc/(1.6 \times 10^{-19}) \text{ [eV]} \\ &= BRc \text{ [eV]} \\ &= BRc/10^9 \text{ [GeV]} \\ \therefore p_T &= BRc/10^9 \text{ [GeV/c]}, \end{aligned} \quad (7)$$

where  $B$  is in Teslas and  $R$  is in metres, and the factor  $c/1e9 = 0.299792458$ . The transverse momentum here means the momentum perpendicular to the direction of the  $B$ -field, which is in the  $y$ -direction, thus  $p_T = \sqrt{p_x^2 + p_z^2}$ .

The radius of curvature of the track within the  $B$ -field is calculated using the angles of the upstream  $\theta_{in}$  and downstream  $\theta_{out}$  portions of the track, and the distance over which the field is present, as:

$$R = \frac{L}{\sin \theta_{in} - \sin \theta_{out}}, \quad (8)$$

where the angles  $\theta_{in}$  and  $\theta_{out}$  have been corrected for the magnet's own rotation (see geometry section) such they are in the magnet's frame of reference.  $L = 1.0668\text{m}$  is the distance over which the field is present, not the full length of the magnet itself.

The magnetic field is known, and the  $p_T$  is thus measured. The remaining step is to use the slope of the track (in the  $y - z$  plane) to find the momentum:

$$p = \frac{p_T}{\cos \beta}, \quad (9)$$

where  $\beta = \tan^{-1} b$  and  $b$  is the track slope as defined in the previous section.

### 3.4 Correct the approximated momentum for magnetic field variations

The magnetic field is not uniform, as shown by the studies of Lackey & Messier using the magnetic field maps of Torun. A correction scale factor  $c_B(\mathbf{r})$  is therefore applied based on the transverse distance in metres between the track's entry to the magnetic field region,  $\mathbf{r}$ , as:

$$c_B(\mathbf{r}) = (\alpha_1 + \alpha_2 \mathbf{r}) \left( \frac{1}{1 + e^{(\mathbf{r}-\alpha_3)/\alpha_4}} - \frac{1}{1 + e^{(\mathbf{r}-\alpha_5)/\alpha_6}} \right) \quad (10)$$

where the parameters are in the correction are

$$\begin{aligned} \alpha_1 &= 1.00068819 \\ \alpha_2 &= -0.04635663 \\ \alpha_3 &= 0.11454936 \\ \alpha_4 &= 0.00971984 \\ \alpha_5 &= -0.11526033 \\ \alpha_6 &= 0.01645662 \end{aligned} \quad (11)$$

More detail on this correction can be found in REF.

### 3.5 Calculating the intersections between the magnet front face and the upstream track

The magnet's x-axis is rotated in the xz plane by 8 degrees, such that a line passing through the front face of the magnet can be extrapolated back to the global x-axis at  $z_0$  (the z-position of the target). This allows us to write down the straight line formula for the magnet's x-axis in global coordinates:

$$x = mz + x_0, \quad (12)$$

where  $m = \frac{dx}{dz}$ , and equivalently the straight line for the upstream track:

$$x' = m'z' + x'_0, \quad (13)$$

such that the intersection between the track and the magnet's front face may be found by requiring  $x = x'$  and  $z = z' = \mathbf{z}$ :

$$m'\mathbf{z} + x'_0 = m\mathbf{z} + x_0, \quad (14)$$

such that the z-position where track and magnet front face intersect is given by:

$$\mathbf{z} = \frac{x'_0 - x_0}{m - m'} \quad (15)$$

It then follows that the x-position where the track intersects the magnet front face is given by:

$$\mathbf{x} = m\mathbf{z} + x_0 \quad (16)$$

## 4 Validation of the new implementation of WCTrackAlg

All of the WCTrack properties' distributions are shown in Figure 12 for all data collected across periods 2, 3, and 4 with both positive and negative magnet polarities with a current of 1000 Amps. A comparison is given between the new (green) and original (black) implementations of the WCTrackAlg, with 4 wirechamber hits required. In both cases, the recent updated geometry is used.

Figure 12a shows the transverse distance between the track and the magnet's center, which is used as the parameter in the correction to the momentum for magnetic field non-uniformity. The new implementation is skewed towards positive x as expected, as a track going directly down the collimated tertiary beam z-axis will enter the rotated magnet at 7.4 cm ( $L/2 \sin(8^\circ)$  where L is the magnet effective length=106.68cm). **The studies by Lackey and Messier indicate that a transverse magnet distance greater than around 8cm does not elicit a reliable momentum correction. This indicates that a symmetric distribution was expected?**

Figure 12b shows the momentum in MeV. This is peaked roughly around 1000 MeV as expected for a magnet current of 1000 Amps. The new implementation is less symmetric, and has fewer tracks at higher momenta. The new implementation without the magnetic field non-uniformity correction is shown in dashed red, confirming that the correction is the primary cause of this curious change in shape. The correction is parametrised by the transverse magnet distance, with a larger distance resulting in a larger momentum correction.

Figure 12c shows the difference in the angles ( $dy/dz$ ) between the upstream and downstream parts of the reconstructed track. We don't expect any notable slope in the y-z plane, as the magnetic field has no effect in the y-direction. I am not sure why this is an interesting property, but it is reassuring that it is very small.

Figure 12d shows the average residual from the points used for the track. The definition for the new implementation is slightly different from the original, which used a different normalisation ( $1/\sqrt{n}$ ) and applied a cut of 12cm on the average. The new implementation required each individual residual to be less than 12cm (ie within the wirechambers) and normalises by the number of points ( $1/n$ ).

Figure 12e and Figure 12f show the projected x and y positions of entry to the NOvA front face, relative to the NOvA front face center. The projection is done using the downstream portion of the track. The y-distribution peaks around -8cm because of the vertical positioning of the detector with respect to the beamline.

Figure 12g and Figure 12h show the x and y position of entry to the magnet front face. **I have no idea why the original implementation is peaked at positive 20cm in x and negative 8cm in y. Additionally, the z-distribution is peaked at -1040 cm, very strange indeed, particularly as the transverse magnet distance is  $\sqrt{x^2 + z^2}$  and somehow comes out at the expected values.**

Figures 12i -12k show the x, y, z components of the unit vector representing the direction of the downstream track. These look as expected, with almost all of the tracks' directions being in z. Figures 12l is the angle of the downstream track in the xz plane, relative to the z-axis, and Figure 12p is the angle in the xy plane, relative to the x-axis. **The phi distribution peaks at  $-\pi, 0, \pi$ ; this indicates tracks are either pointing along the x-axis at zero (directly left) or opposite to this (directly right). In other words, the track has a direction in x rather than in y..**

Figures 12m -12o show the difference in the x, y, z intercepts of the upstream and downstream parts of the track with the magnet front face. The original distributions here are apparently nonsensical as they use a magnet midpoint plane position which is not within the beamline instrumentation, as it was hardcoded by Lariat.

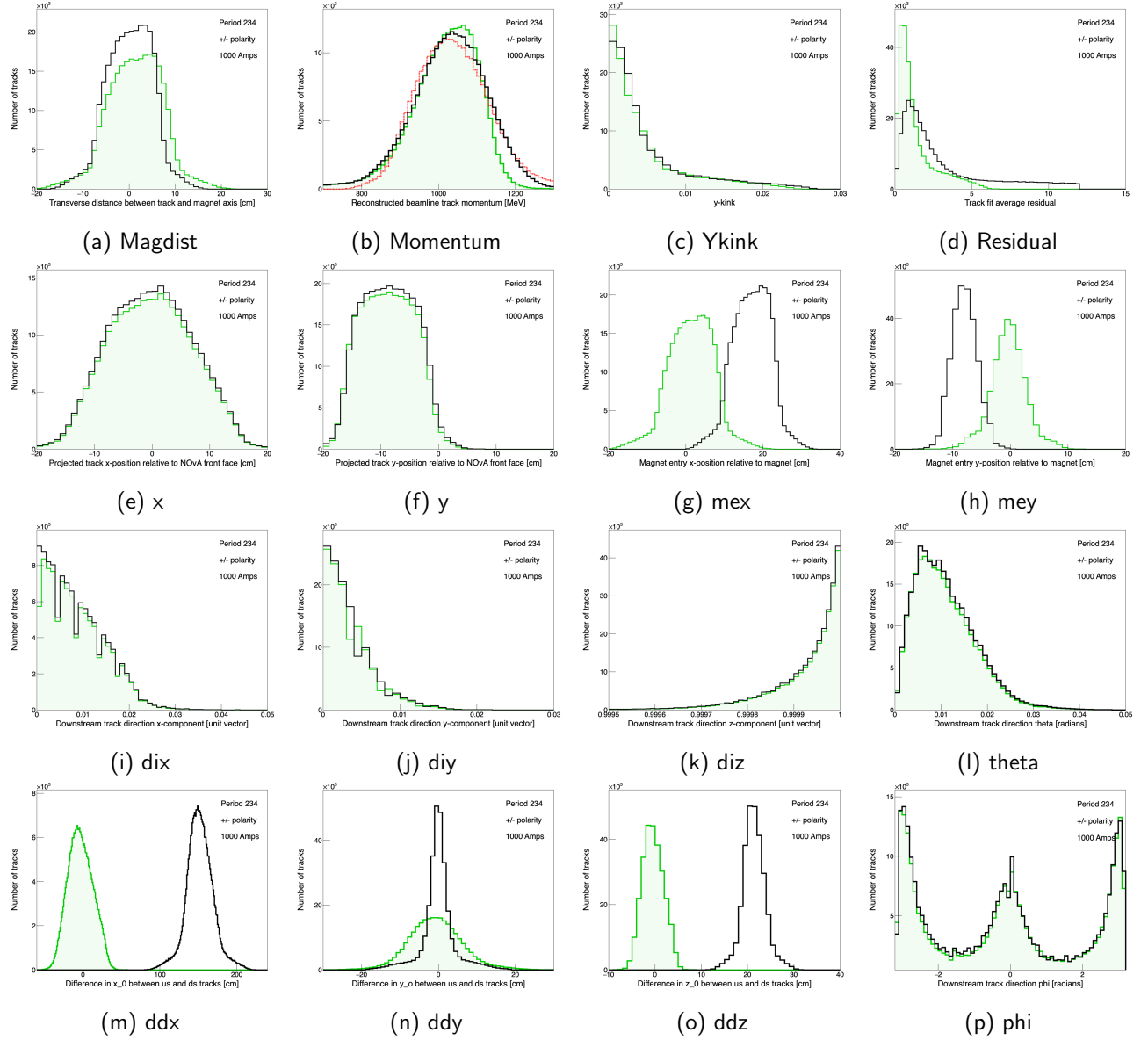


Figure 12: The WCTrack properties. The black unfilled histograms are the original implementation of the algorithm, and the green shaded histograms are for the new implementation.

## 4.1 Counting tracks of each type

First up we want to compare the counts of different types of tracks in the different regions. These counts are visualised in Table 1. Two things to note:

1. There are notably more 3 point tracks (no wc2) in period 4 than in period 3.
2. Within period 4, there are notably more 3 point tracks (no wc2) and (no wc4) when the magnet polarity is set to negative.

Magnet current	500	750	1000	1250
Original Track	█	█	██████	
New 4 point track	█	█	██████	
3 point (no wc2)	█	█	█	
3 point (no wc3)	█	█	█	
3 point (no wc4)	█	█	█	

(a) Period 2, positive polarity. N=8009.

Magnet current	500	750	1000	1250
Original Track	█		██████	
New 4 point track	█		██████	
3 point (no wc2)			█	
3 point (no wc3)			█	
3 point (no wc4)			█	

(b) Period 2, negative polarity. N=382.

Magnet current	500	750	1000	1250
Original Track	████	████	████	
New 4 point track	████	████	████	
3 point (no wc2)	█	█	█	
3 point (no wc3)	█	█	█	
3 point (no wc4)	█	█	█	

(c) Period 3, positive polarity. N=5995.

Magnet current	500	750	1000	1250
Original Track	█		██████	
New 4 point track	█		██████	
3 point (no wc2)			█	
3 point (no wc3)			█	
3 point (no wc4)			█	

(d) Period 3, negative polarity. N=1825.

Magnet current	500	750	1000	1250
Original Track	█	█	██████	█
New 4 point track	█	█	██████	█
3 point (no wc2)	█	█	█	█
3 point (no wc3)	█	█	█	█
3 point (no wc4)	█	█	█	█

(e) Period 4, positive polarity. N=13082.

Magnet current	500	750	1000	1250
Original Track	████	████	██████	█
New 4 point track	████	████	██████	█
3 point (no wc2)	████	████	██████	█
3 point (no wc3)	█	█	█	█
3 point (no wc4)	█	█	█	█

(f) Period 4, negative polarity. N=3600.

Table 1: Counts for the different track types sub-divided by data taking period, magnet polarity, and magnet current in Amps. The maximum data bar scale in each case is given by N = number of tracks.

The reader may find it easier to visualise using Figure 13.

Figure 14 and Figure 15 show the intensity and run number distributions.

When the magnet polarity is set to negative, only negatively charged particles (predominantly pions) are permitted to continue through the magnetic field region in the direction of the downstream wirechambers 3 and 4 and baby NOvA. There is no reason I can think of that would make a change in the magnet's polarity result in wirechamber 2 or 4 being less efficient. The negative polarity runs were not grouped together in time (if they were, one might suspect a degrading performance of WC over time).

My plan to explore this further was to make plots of the hit positions within each wire chamber for negative and positive polarity; these are shown in Figure 7 and don't indicate any polarity-related differences between the wirechambers' performance. So I went back to thinking about what other conditions were related to the polarity differences.

I concluded that there is no correlation between polarity and WC performance - gave a talk on it late April. add a para on that.

## 4.2 Comparing track properties

All of the original WCTrack properties have been kept to ensure back-compatibility. They are as follows:

**WCTrack.Momentum()** The reconstructed momentum corrected for magnetic field non-uniformity. Figure 13 shows the momentum distributions for the 1000 Amp magnet current setting in the three periods for positive and negative polarity settings. I do not understand why the momentum distribution of the New 4 point tracks is skewed to higher momentum than the Original, which looks Gaussian. Want to add the un-corrected momentum distribution to see how much of the difference is coming from the geometry change. May actually be the only explanation.

**WCTrack.TransDistToMagAxis()** Transverse distance from WC track intercept to central axis of magnet. Figure 16 shows the distributions for the 1000 Amp magnet current setting in the three periods for positive and negative polarity settings.

**WCTrack.YKink()** Angle difference dy/dz between upstream and downstream tracks. Figure 19 shows the distributions for the 1000 Amp magnet current setting in the three periods for positive and negative polarity settings.

**WCTrack.Residual()** Returns the average residual, indicating the goodness of fit to a linear regression for the points used in the track. Figure 20 shows the distributions for the 1000 Amp magnet current setting in the three periods for positive and negative polarity settings. Note that the definition of the residual is different in the case of the original WCTrack from the new 4 and 3 point tracks, as described in Section 3.2.

**WCTrack.XYFace** X and Y position of the track on the upstream face of the detector. Figure 21 and 22 show the distributions for the 1000 Amp magnet current setting in the three periods for positive and negative polarity settings.

**WCTrack.DeltaDist()** Distance between upstream and downstream track ends. The x, y, z intercepts of both the upstream and downstream portions of each track are calculated, and the difference between upstream and downstream is the DeltaDist. Figure 23 shows a notable difference in the original tracking algorithm, which is centred around 150cm, and the new implementation which is centred around zero. The track is expected to be diverted in the x-direction due to magnetic field, so I do not understand why the new implementation gives a distribution around zero. [check the implementation of DeltaDist](#). The y-distribution in Figure 24 also shows a difference, with the delta dy distribution being more sharply peaked in the original WCTrack implementation. In this case though both the original and new implementations have a delta dy peaking about zero, which is what I would expect. Finally the delta dx distribution shown in Figure 25 echoes the delta dx distribution differences, but in this case the original delta dz distribution is shifted by just over 20cm. I don't understand this.

**WCTrack.MagnetEntryPoint()** X,Y,Z intersect of upstream WC track with front face of magnet X, Y, Z.

**WCTrack.WCHit()** Hits on each chamber used to make the track WCHit()[0].X()

**WCTrack.Dir()** Unit vector describing direction of downstream track.

**WCTrack.Theta()** Theta defined from the Z axis

**WCTrack.Phi()** Phi defined counterclockwise from the X axis

**WCTrack.WCMissed()** Integer corresponding to the number of the wirechamber with no hit.

## 5 Considerations for analysers

Usual quality cuts are on Residual, TransDistToMagAxis, YKink.

In addition the analyser might want to cut on WCMissed.

[Several things to add here](#)

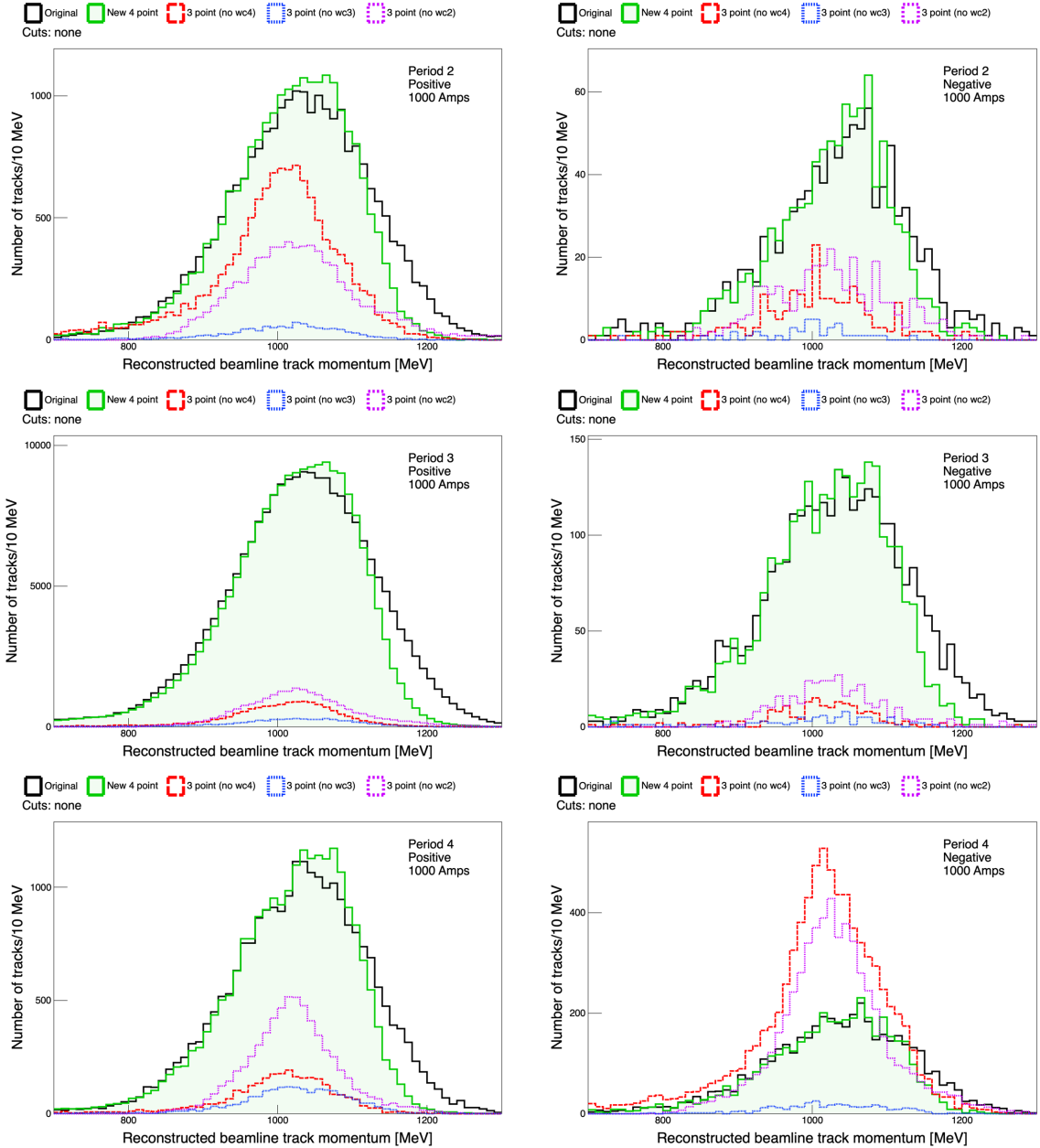


Figure 13: The WCTrack momentum with magnet current 1000 Amps. Left: positive polarity, Right: negative polarity, Top: period 2, Center: Period 3, Bottom: period 4. No cuts applied.

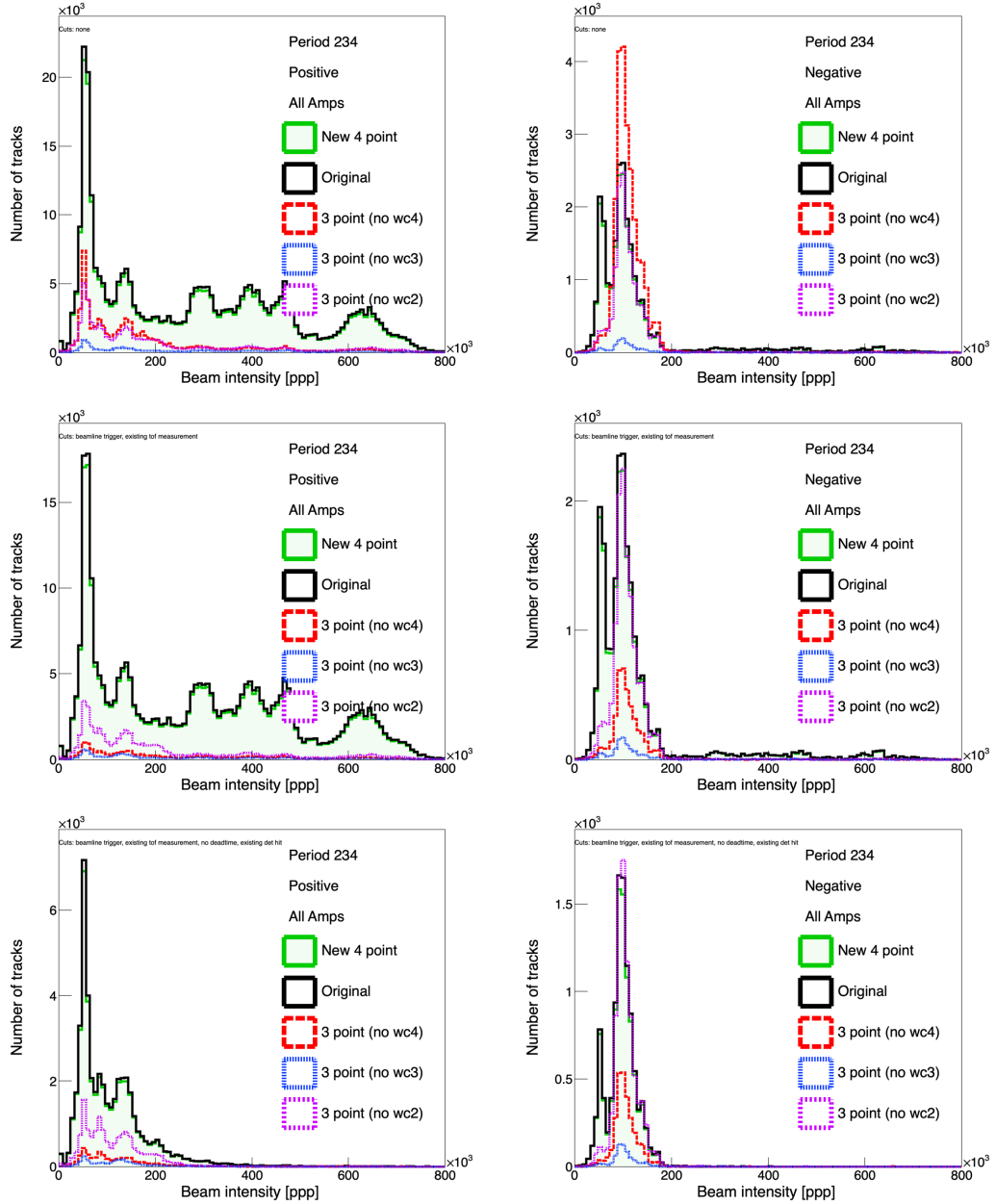


Figure 14: The beam intensity for top: no cuts, middle: trigger and tof cuts; bottom: + deadtime and detector hit cuts. Left is positive polarity, right is negative polarity.

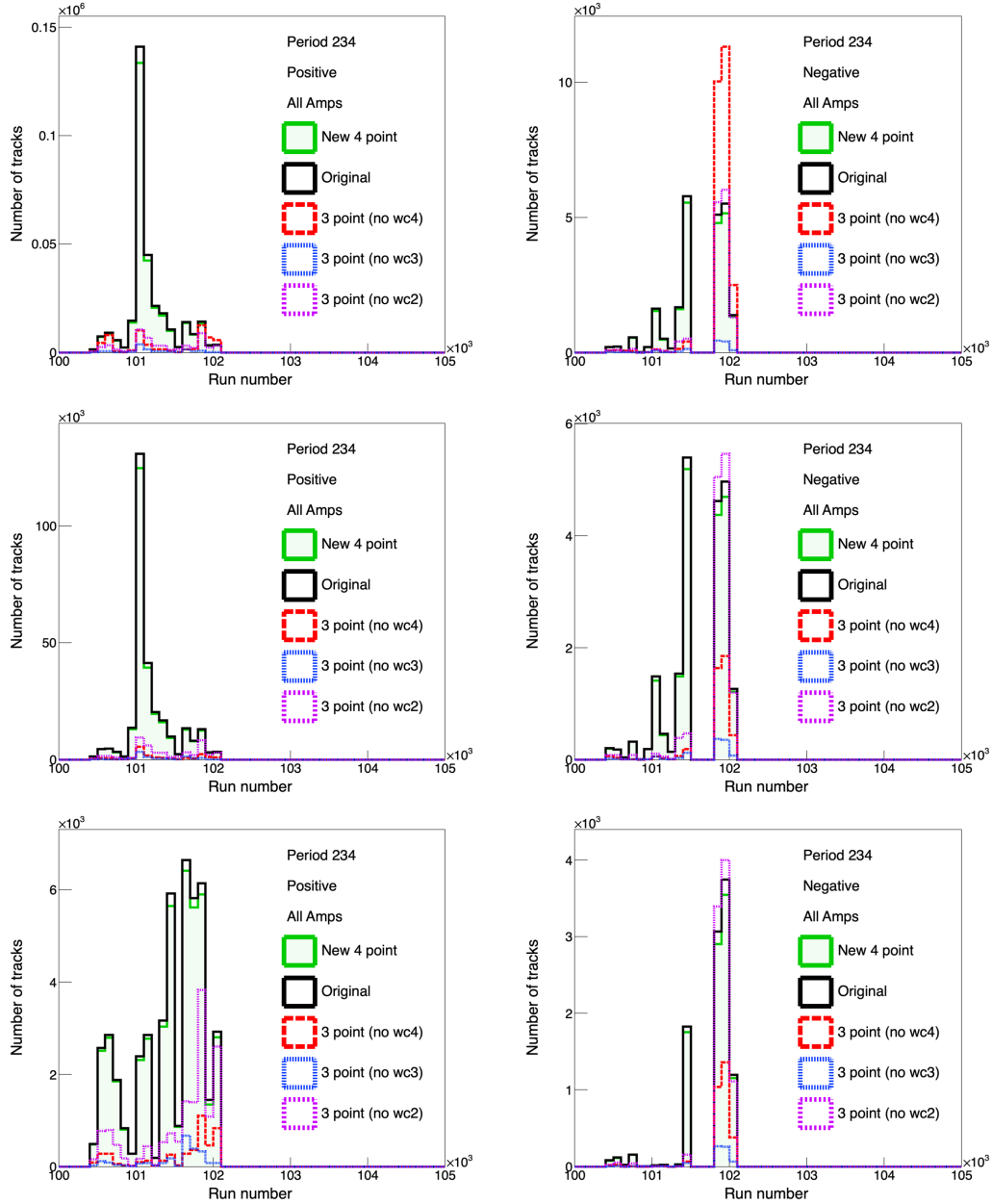


Figure 15: The run number for top: no cuts, middle: trigger and tof cuts; bottom: + deadtime and detector hit cuts. Left is positive polarity, right is negative polarity.

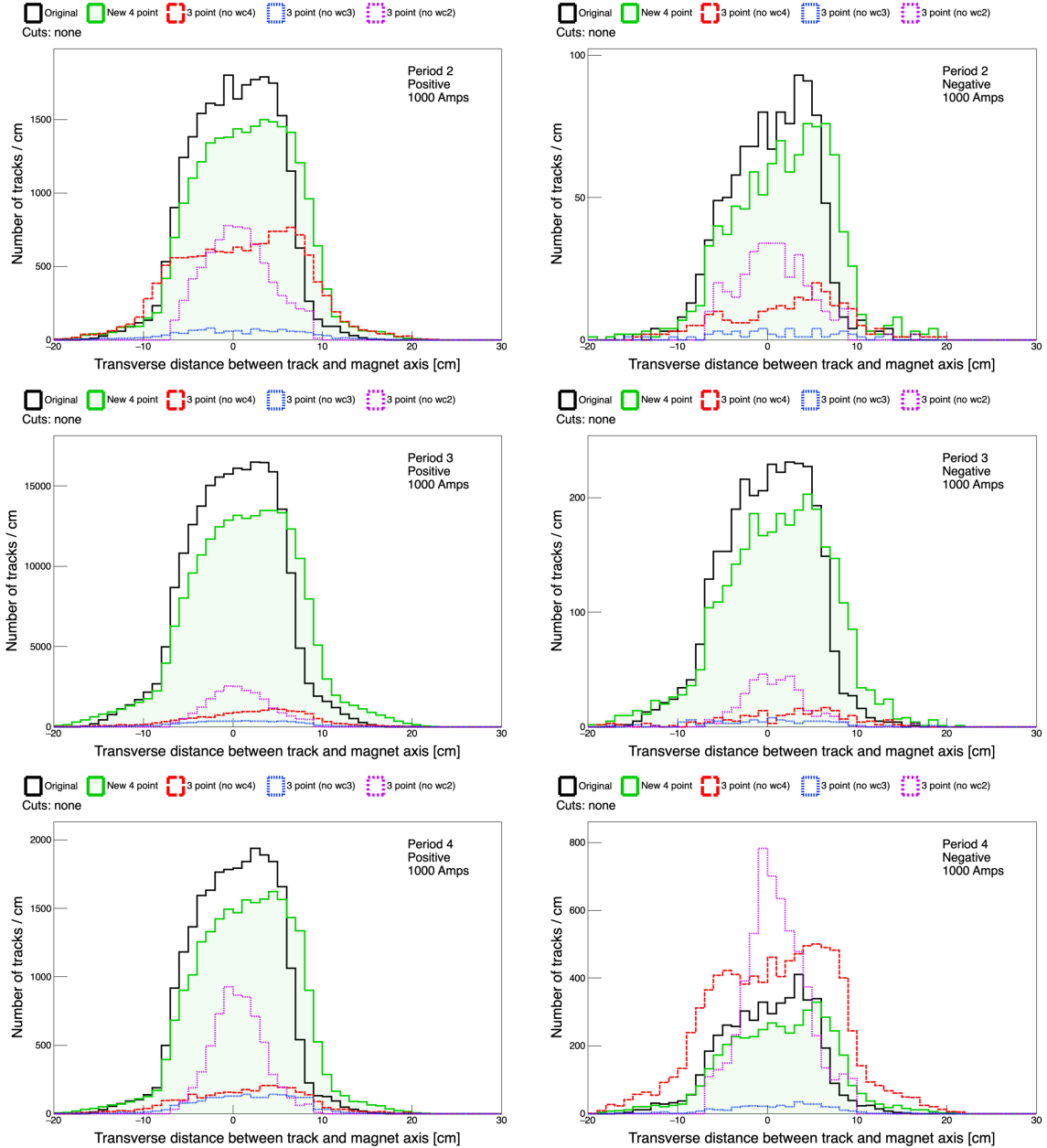


Figure 16: The WCTrack magnet distance with magnet current 1000 Amps. Left: positive polarity, Right: negative polarity, Top: period 3, Bottom: period 4. No cuts applied.

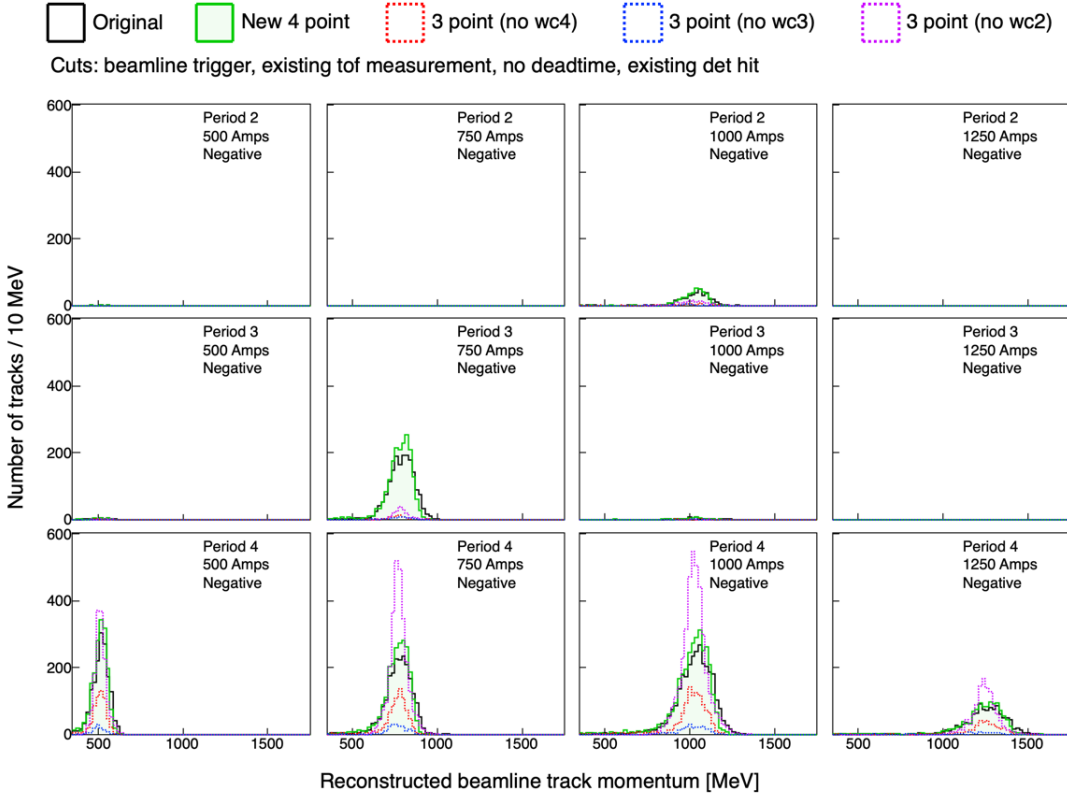


Figure 17: The WCTrack momentum for negative polarity broken down by row: period and column: magnet current setting. There is a common y-axis scale for all plots.

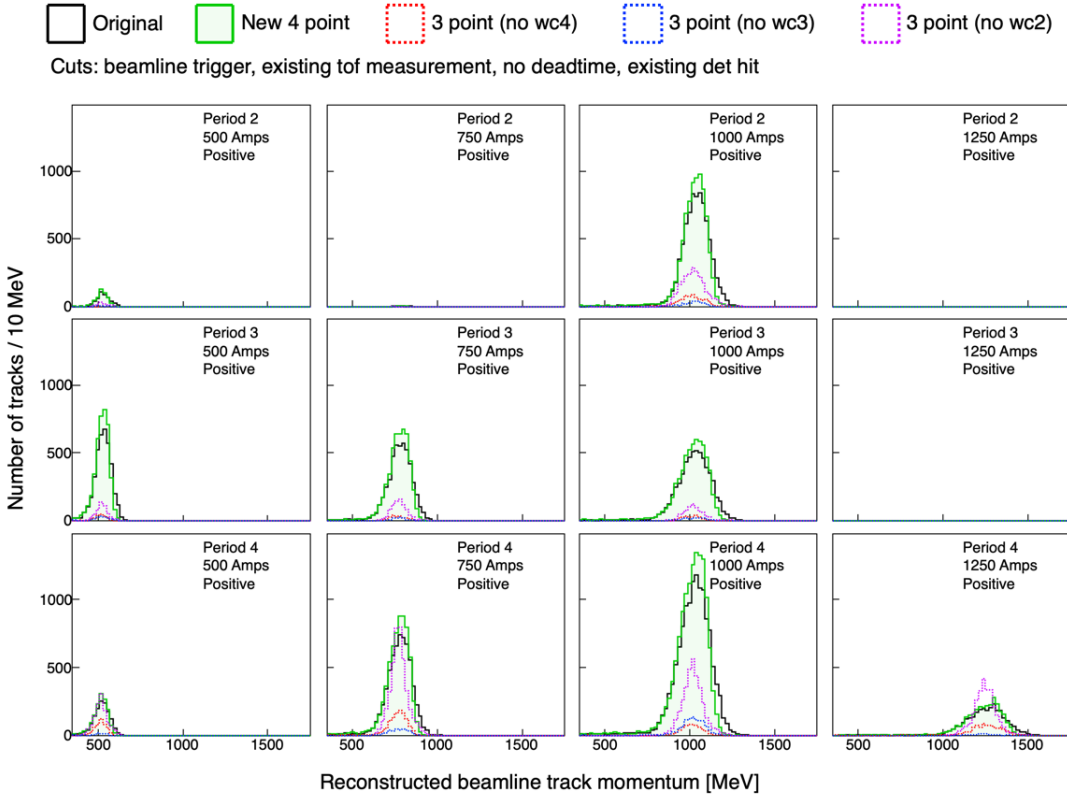


Figure 18: The WCTrack momentum for positive polarity broken down by row: period and column: magnet current setting. There is a common y-axis scale for all plots.

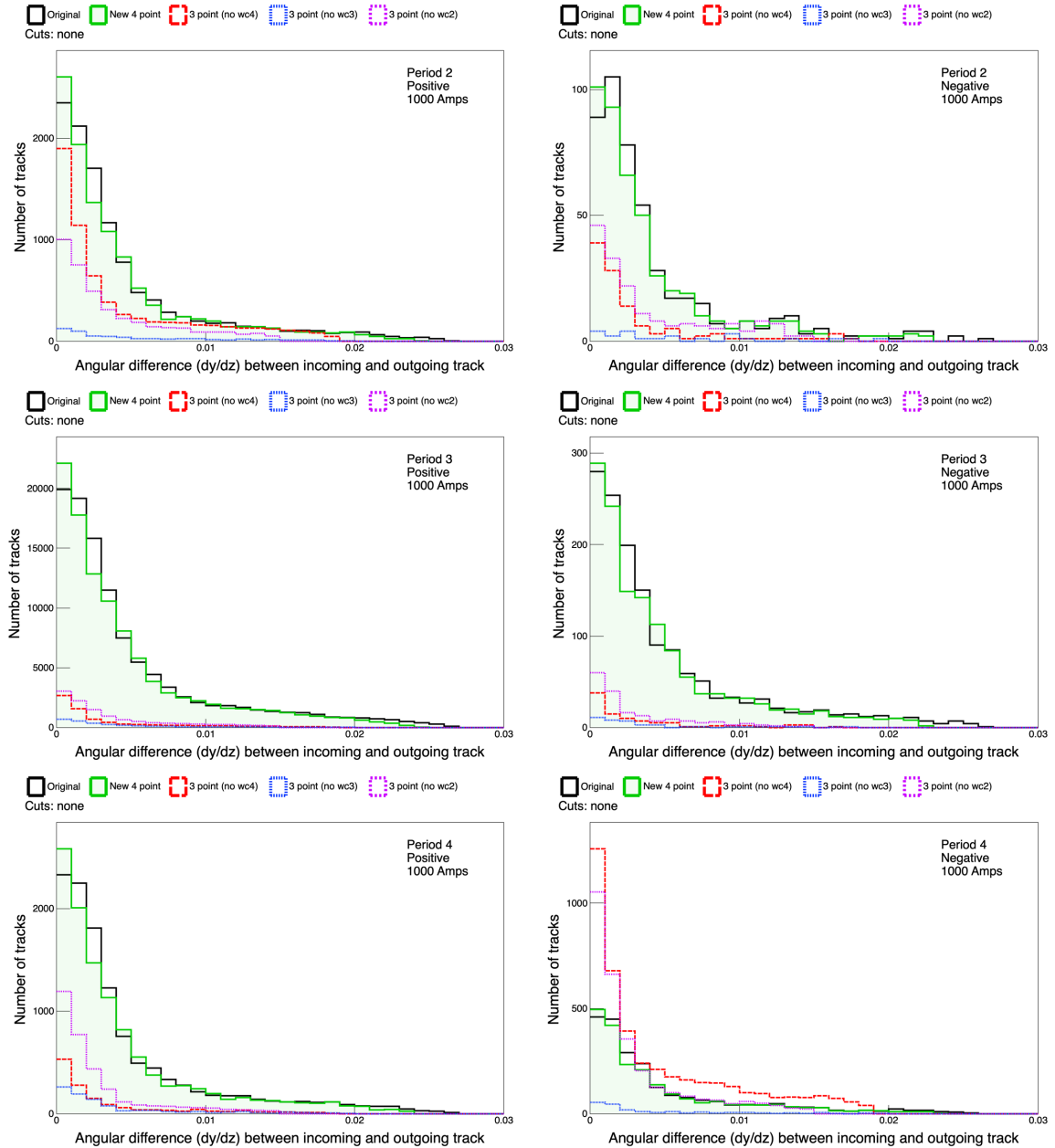


Figure 19: The WCTrack ykink with magnet current 1000 Amps. Left: positive polarity, Right: negative polarity, Top: period 2, Center: period3, Bottom: period 4. No cuts applied.

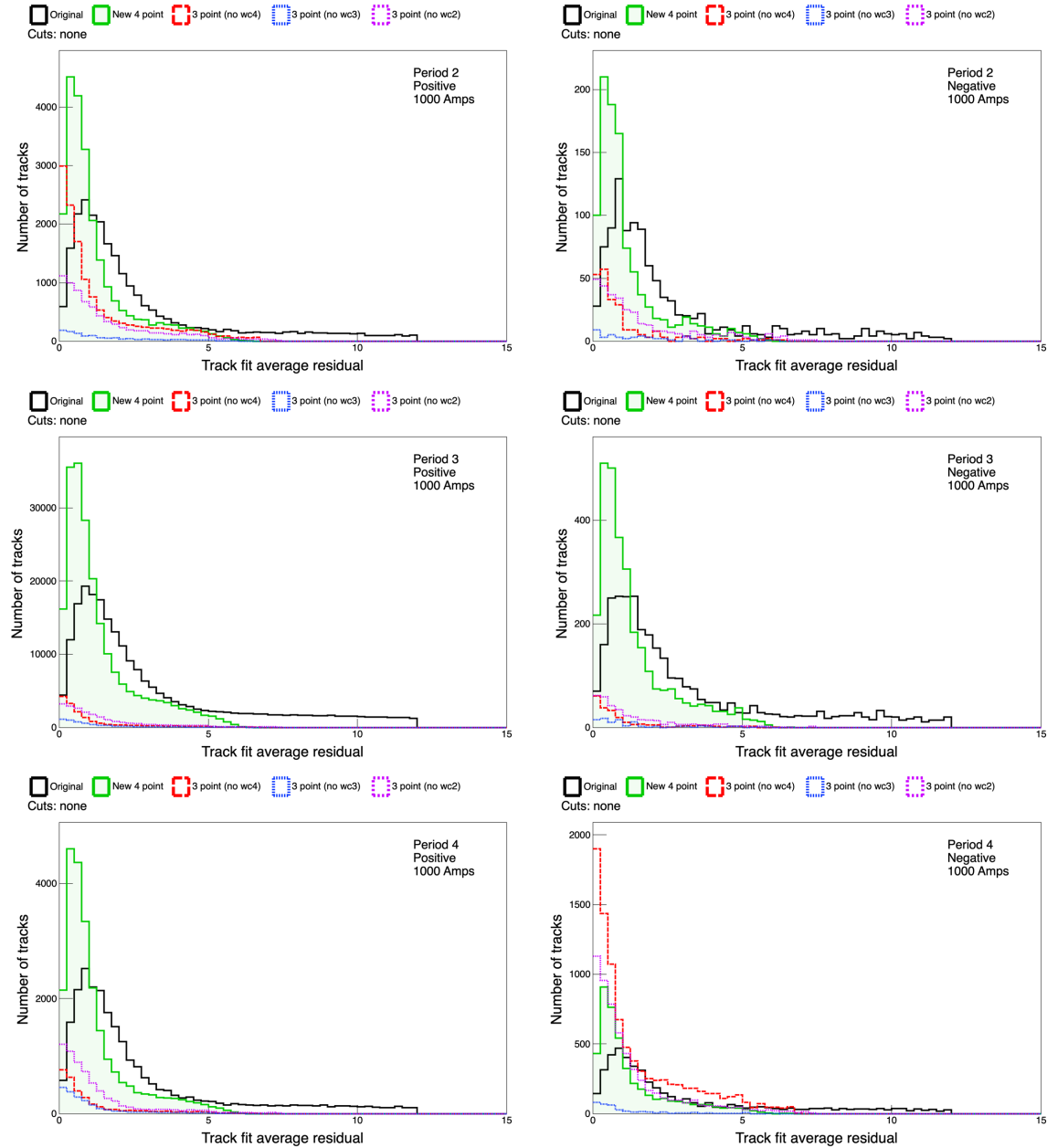


Figure 20: The WCTrack residual with magnet current 1000 Amps. Left: positive polarity, Right: negative polarity, Top: period 2, Center: period3, Bottom: period 4. No cuts applied. .

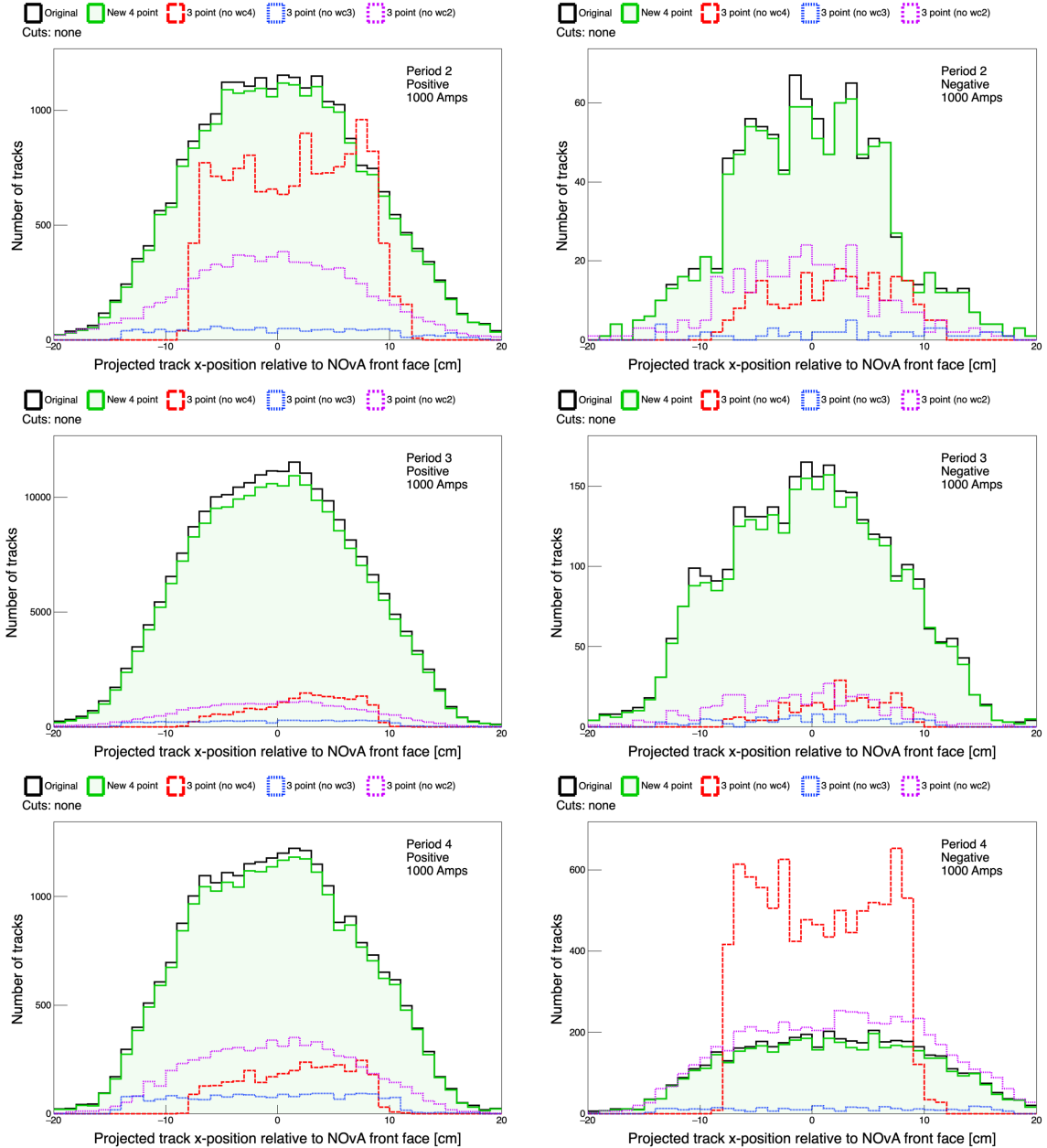


Figure 21: The WCTrack x with magnet current 1000 Amps. Left: positive polarity, Right: negative polarity, Top: period 2, Center: period3, Bottom: period 4. No cuts applied.

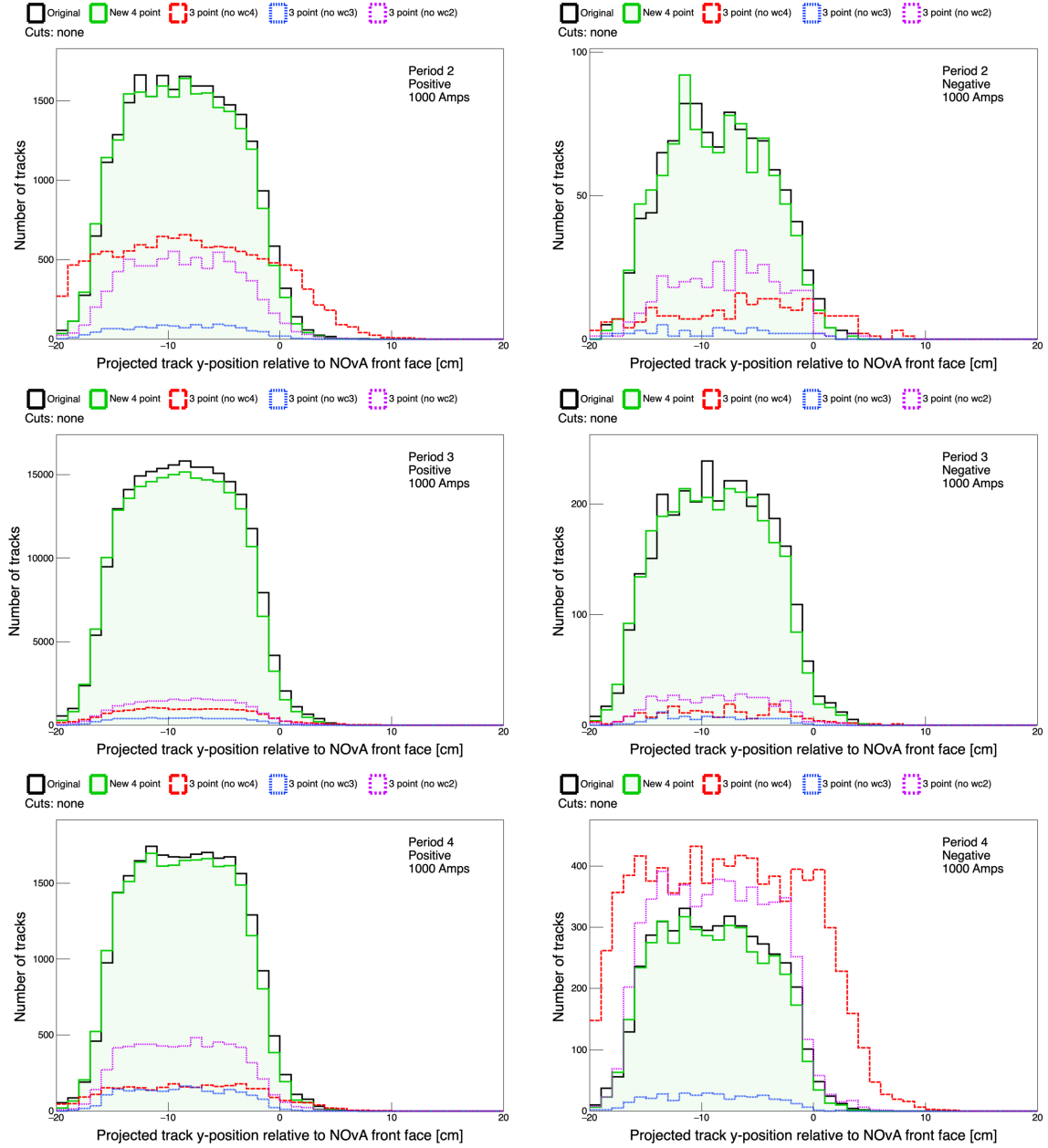


Figure 22: The WCTrack  $y$  with magnet current 1000 Amps. Left: positive polarity, Right: negative polarity, Top: period 2, Center: period3, Bottom: period 4. No cuts applied.

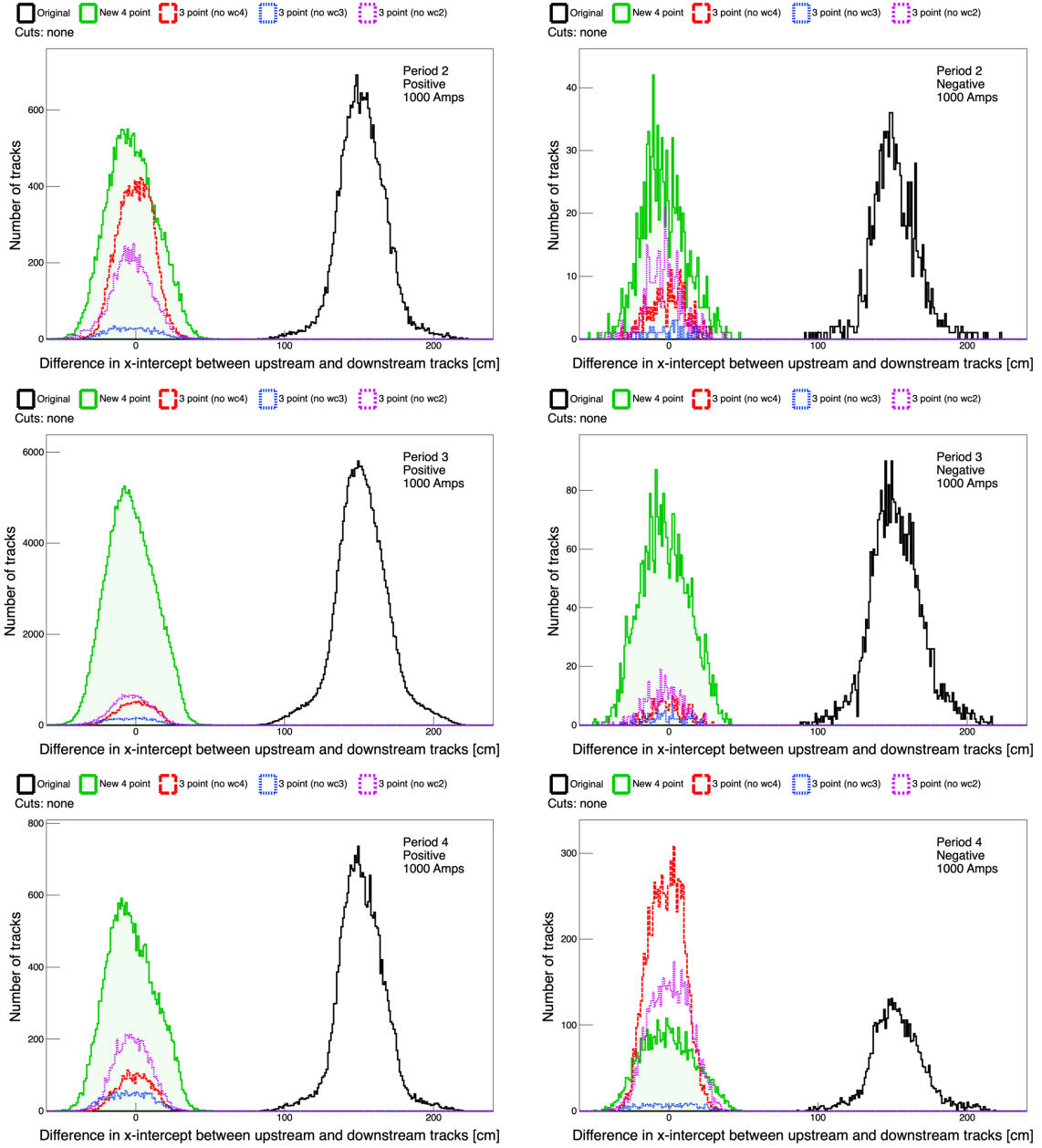


Figure 23: The WCTrack delta dx with magnet current 1000 Amps. Left: positive polarity, Right: negative polarity, Top: period 2, Center: period3, Bottom: period 4. No cuts applied.

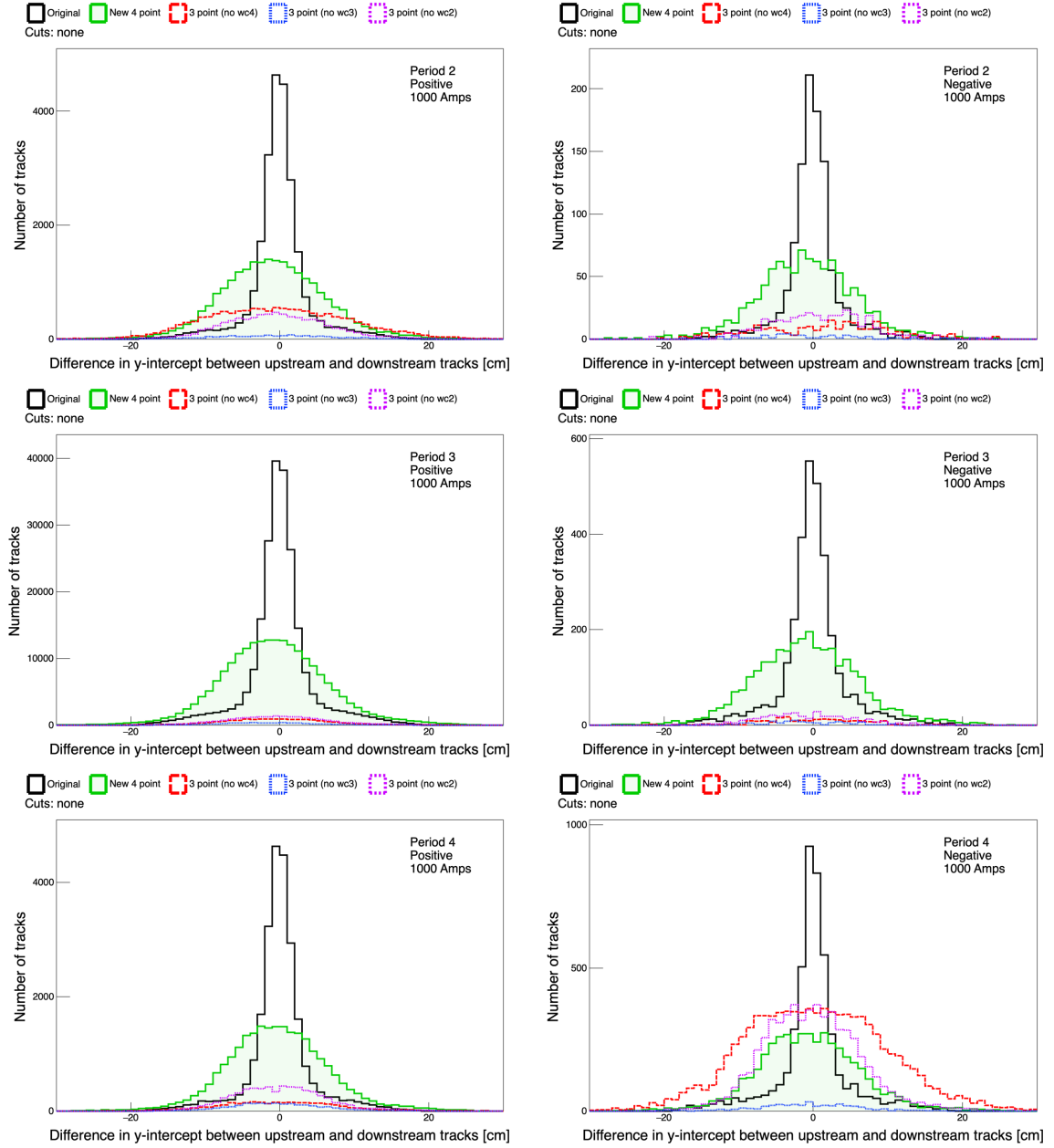


Figure 24: The WCTrack delta dy with magnet current 1000 Amps. Left: positive polarity, Right: negative polarity, Top: period 2, Center: period3, Bottom: period 4. No cuts applied.

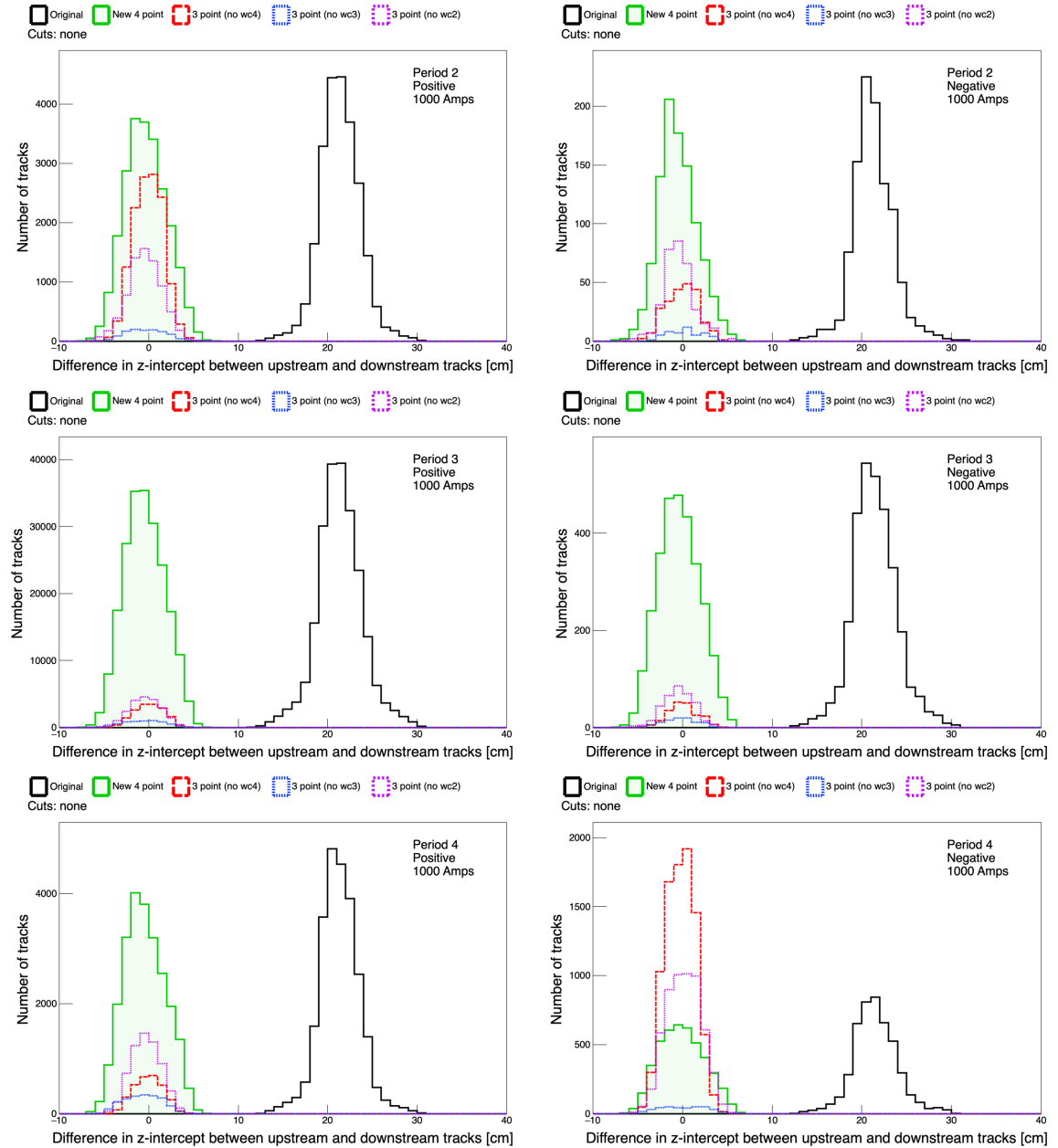


Figure 25: The WCTrack delta dz with magnet current 1000 Amps. Left: positive polarity, Right: negative polarity, Top: period 2, Center: period3, Bottom: period 4. No cuts applied.

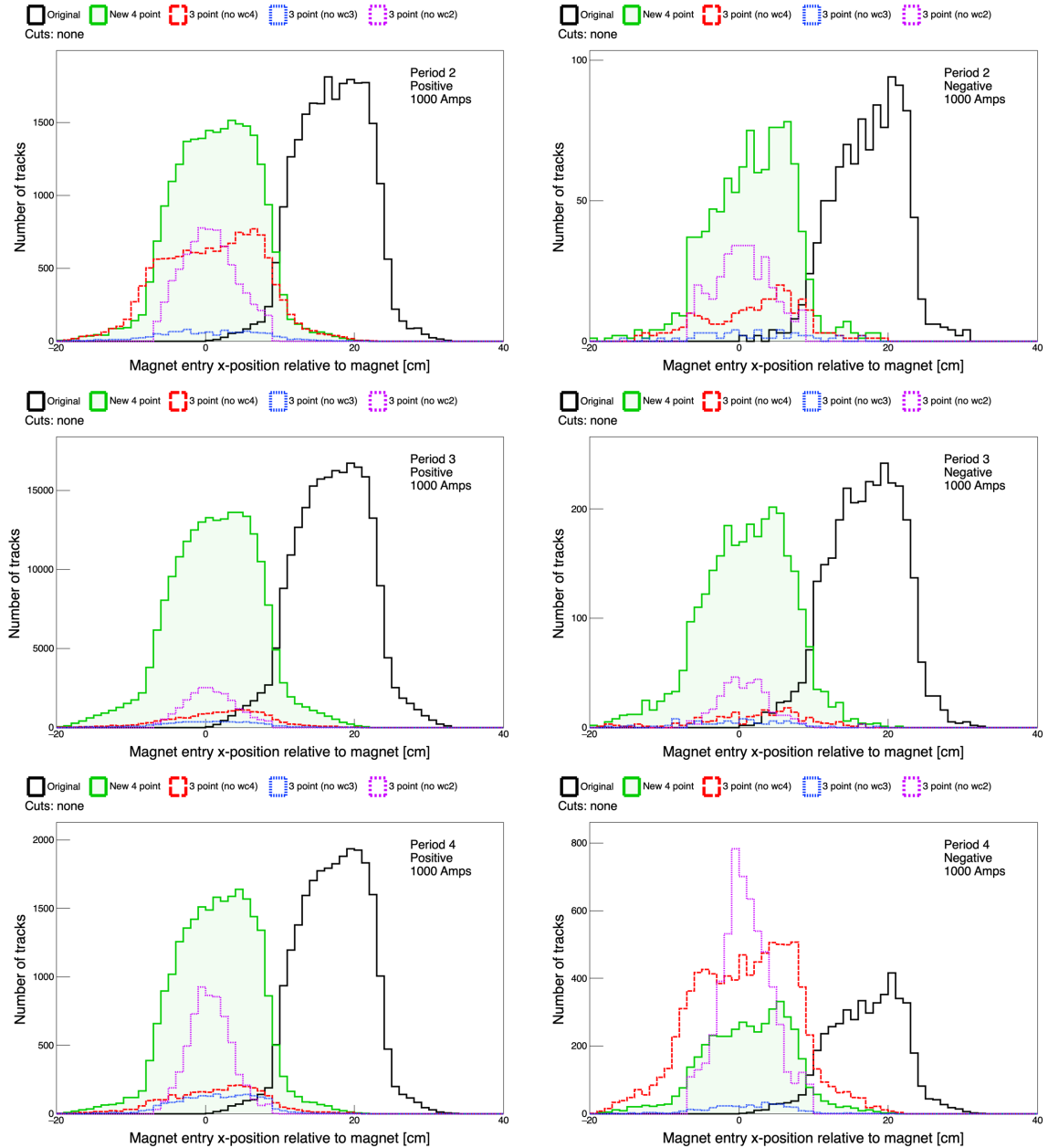


Figure 26: The WCTrack magnet entry x with magnet current 1000 Amps. Left: positive polarity, Right: negative polarity, Top: period 2, Center: period3, Bottom: period 4. No cuts applied.

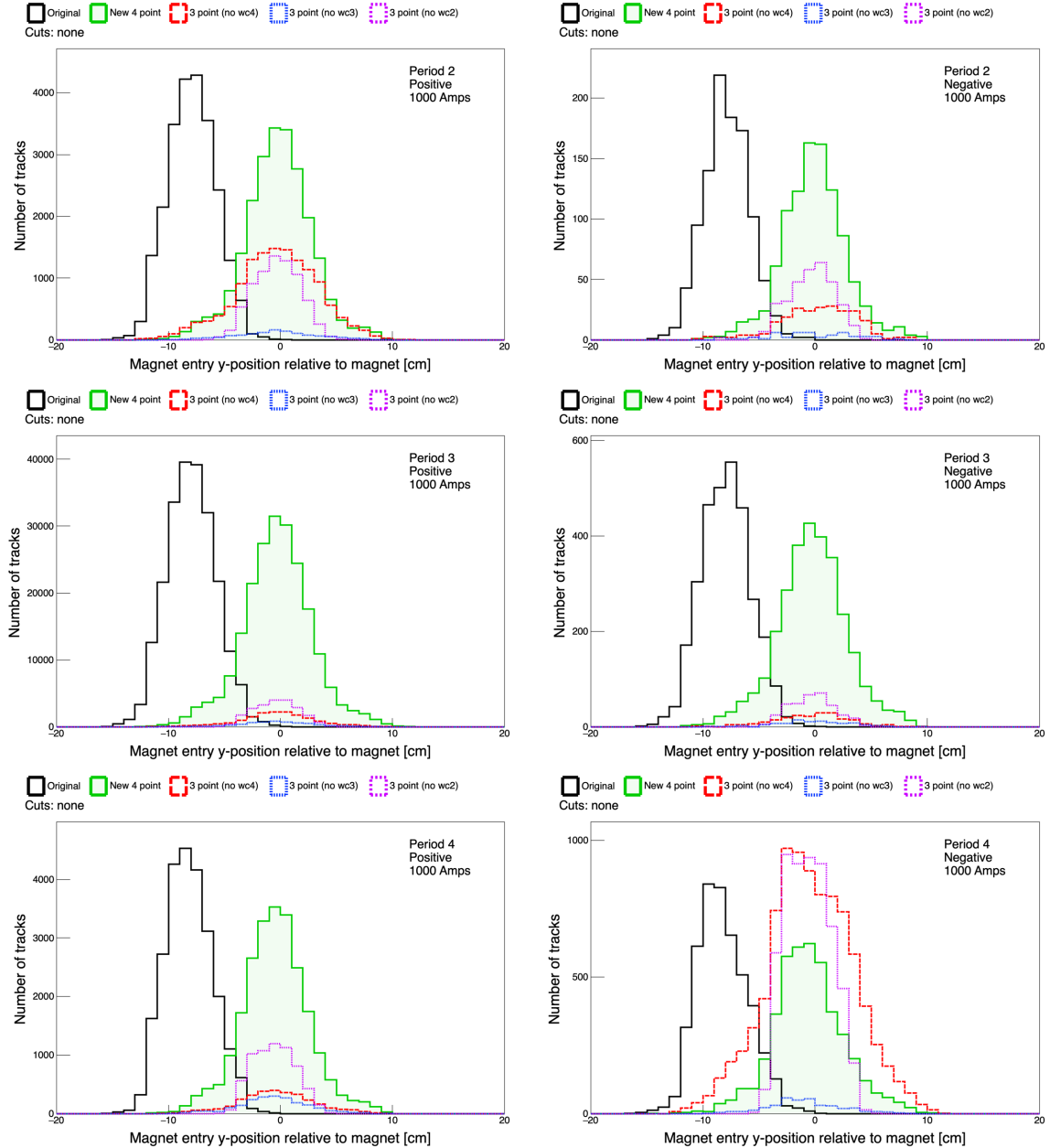


Figure 27: The WCTrack magnet entry y with magnet current 1000 Amps. Left: positive polarity, Right: negative polarity, Top: period 2, Center: period3, Bottom: period 4. No cuts applied.

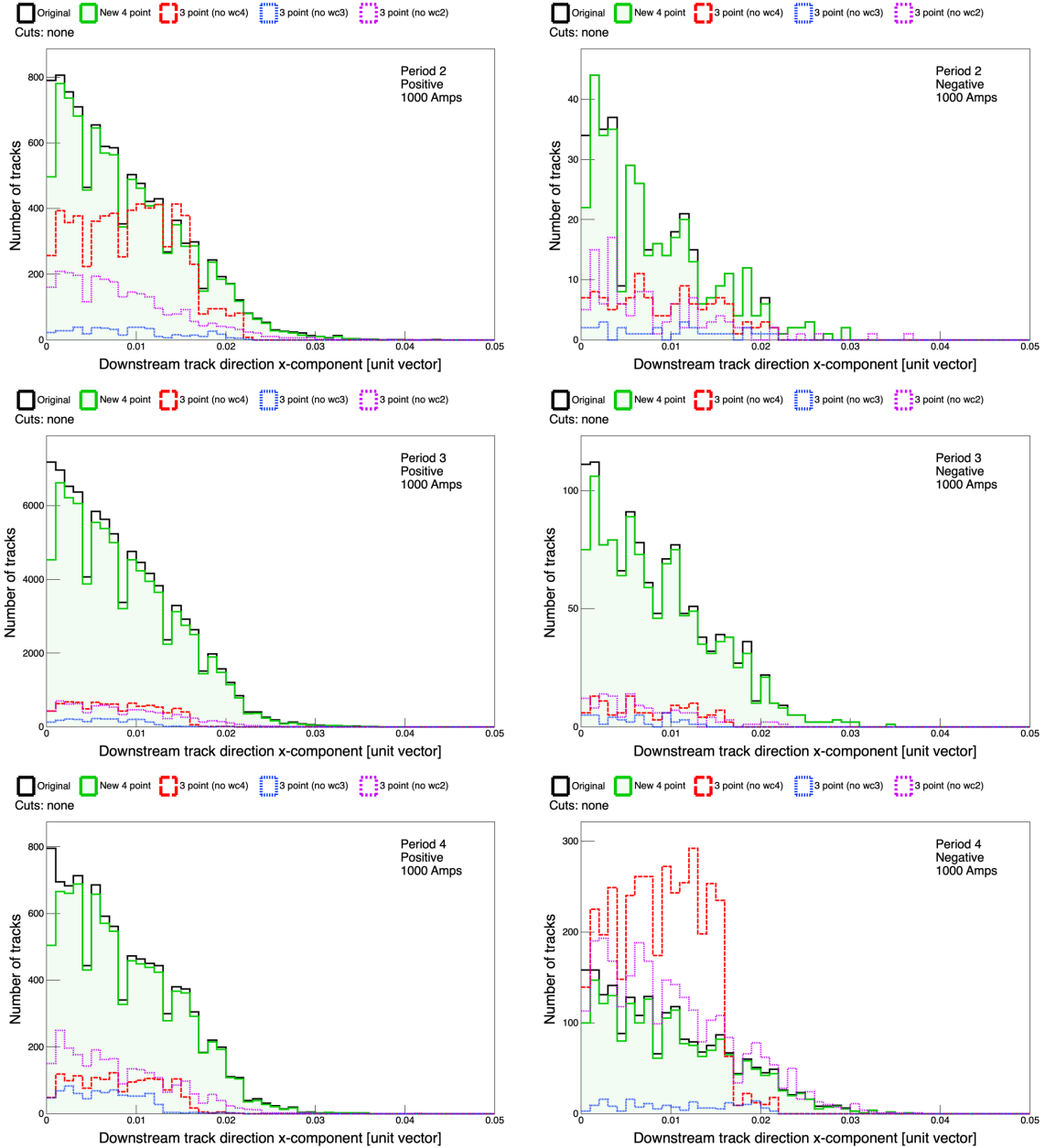


Figure 28: The WCTrack downstream track x-component with magnet current 1000 Amps. Left: positive polarity, Right: negative polarity, Top: period 2, Center: period3, Bottom: period 4. No cuts applied.

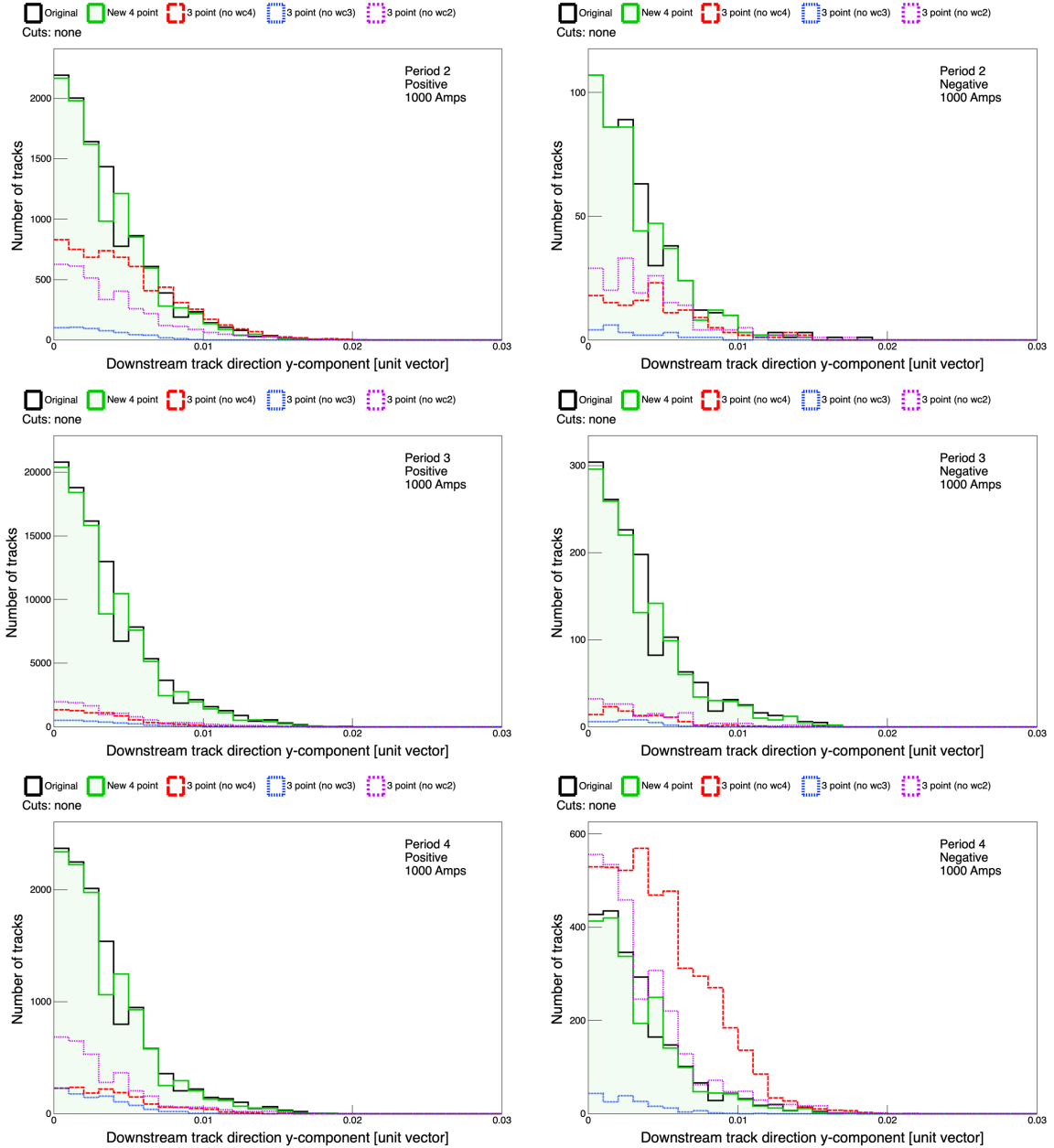


Figure 29: The WCTrack downstream track y-component with magnet current 1000 Amps. Left: positive polarity, Right: negative polarity, Top: period 2, Center: period3, Bottom: period 4. No cuts applied.

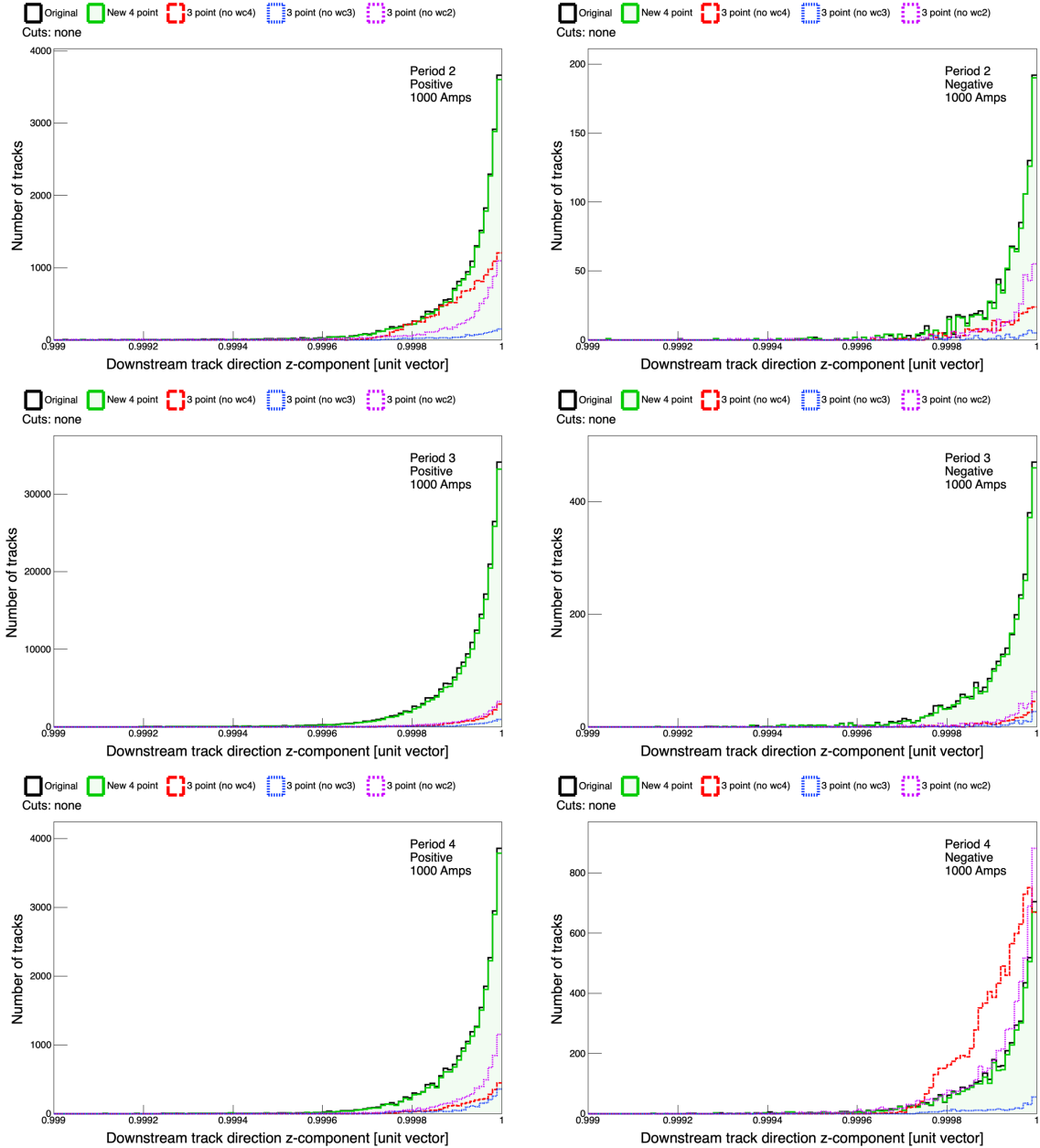


Figure 30: The WCTrack downstream track z-component with magnet current 1000 Amps. Left: positive polarity, Right: negative polarity, Top: period 2, Center: period3, Bottom: period 4. No cuts applied.

## 6 Particle types

Particles can be identified by reconstructing their mass using the momentum measurement from the wire chamber track and the speed  $\beta$  from the time of flight measurement:

$$\beta = d/ct \quad (17)$$

where  $d$  is the distance between the two ToF arms providing a time of flight measurement  $t$  in seconds. During period 2 the ToF arms were 13.1564 metres apart, whereas in period 3 this distance was shortened to 9.70772 metres. The speed of light  $c$  is used to normalise the velocity.

The mass is then

$$m = p/(\gamma * c * \beta) \quad (18)$$

where  $\gamma$  is the Lorentz factor ( $\frac{1}{\sqrt{1 - \beta^2}}$ ) and  $p$  is the momentum as measured using the wire chamber track curvature in the magnetic field.

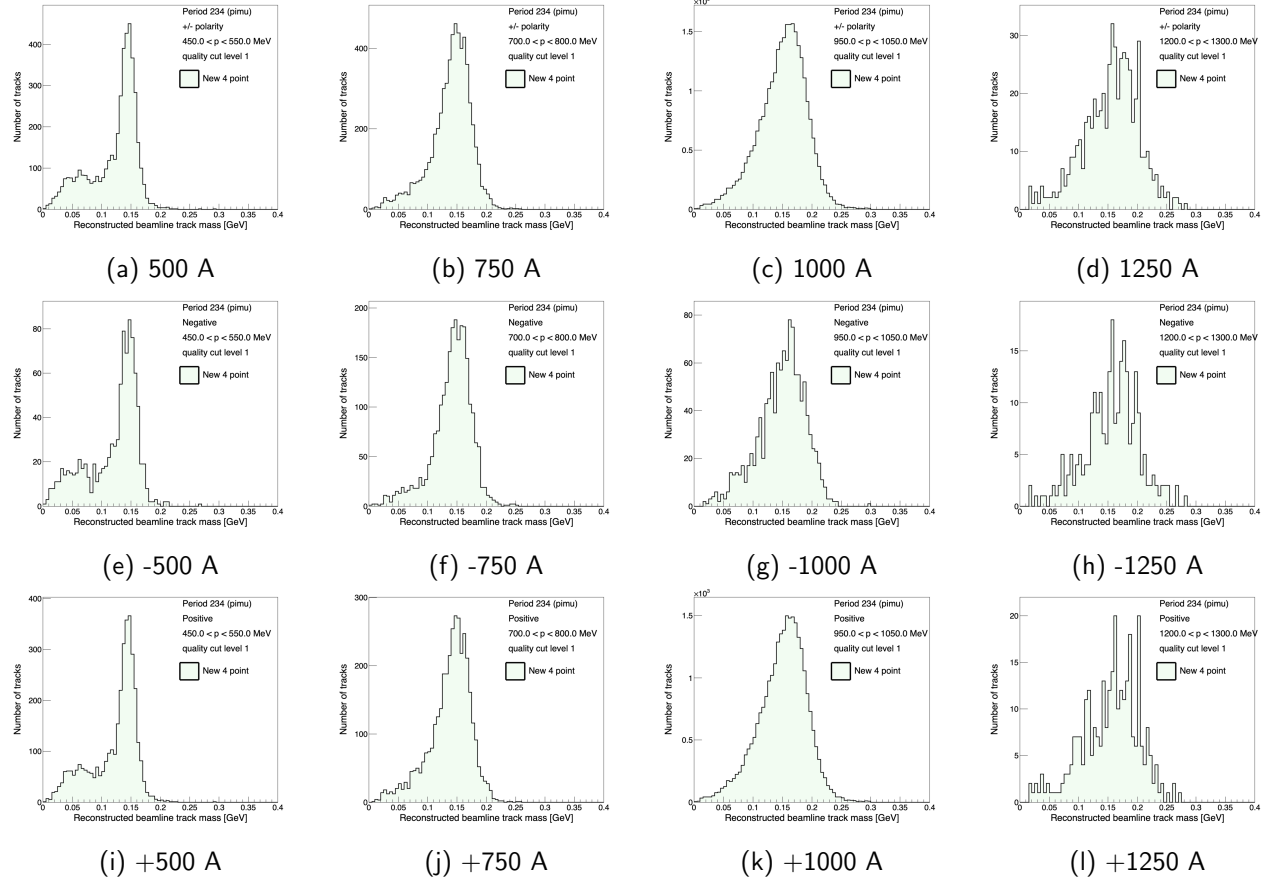


Figure 31: The mass distribution in the region of the pion mass for different magnet current settings shows the distribution widening significantly as the momentum increases. The bottom row shows the distributions with negative polarity. Level 1 means that there are no cuts applied other than the requirement that the momentum is consistent with the magnet current.

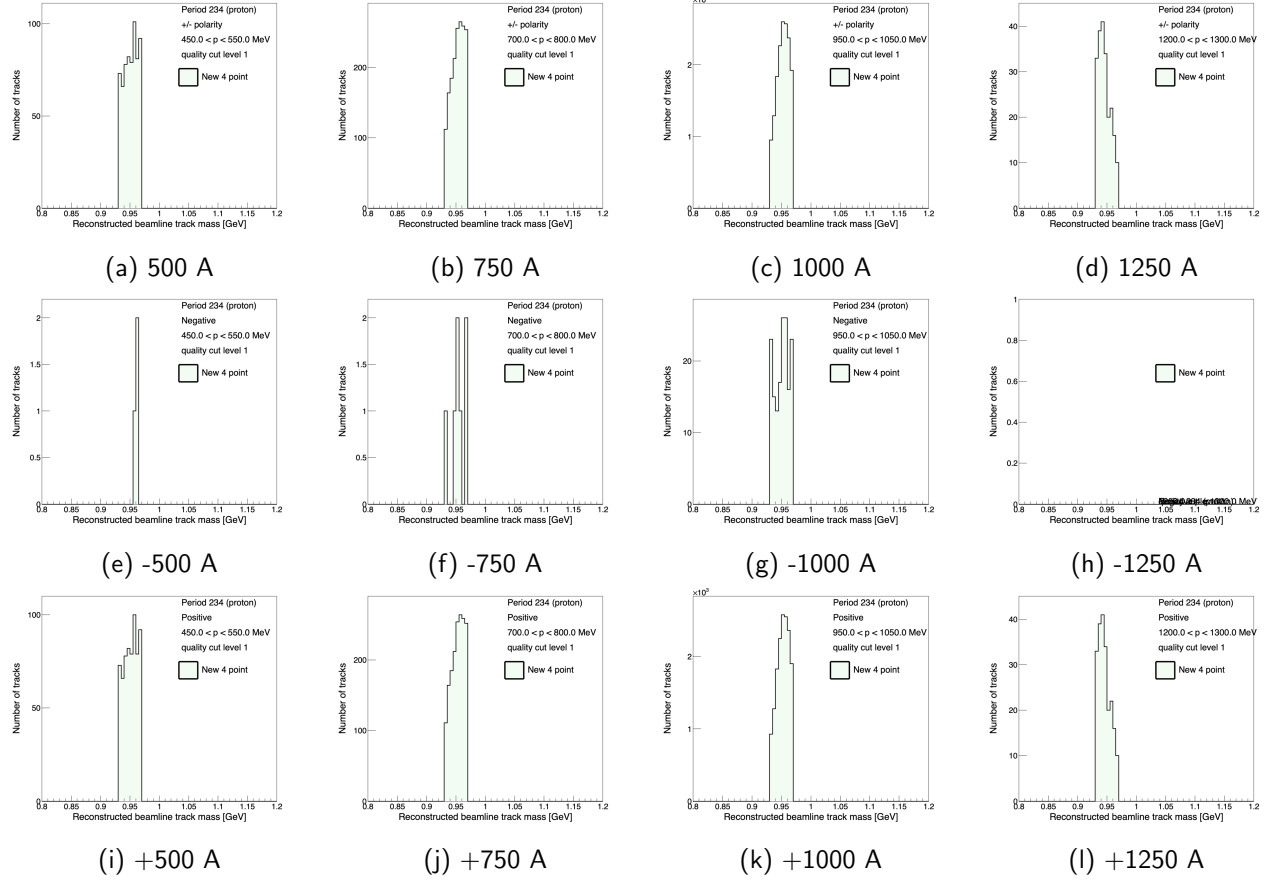


Figure 32: The mass distribution in the region of the proton mass for different magnet current settings. Level 1 means that there are no cuts applied other than the requirement that the momentum is consistent with the magnet current.

## 6.1 Particle speeds

Looking at the particle speeds for different particles can help us to figure out how much we trust the time of flight measurements and is just interesting in its own right.

The kaon speed distribution has two distinct peaks, which is puzzling me. I noticed though that if I add a momentum cut to match the magnet current cut, the lower peak goes away.

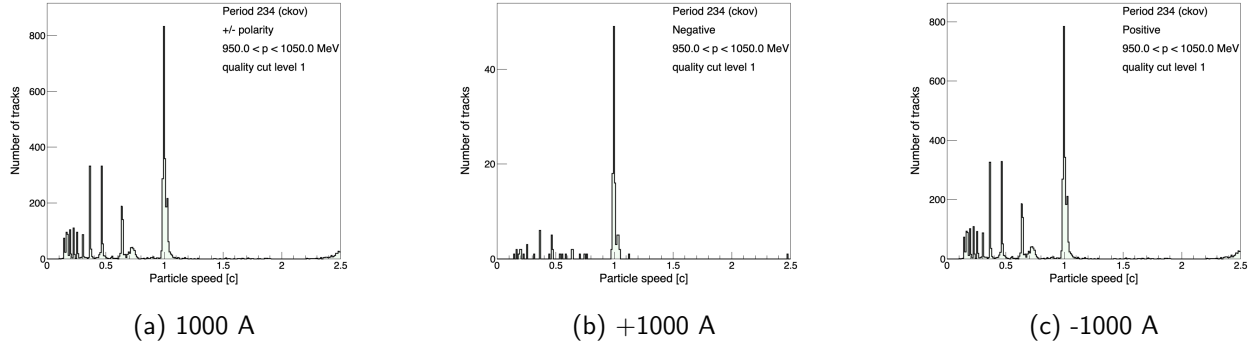


Figure 33: The speed of candidate particles that leave a signal in the threshold cherenkov detector. Everything in the big peak near the speed of light has a negligible wirechamber mass making it likely that these are indeed electrons. The hillock next on the left is consistent with the proton mass, something is happening between the proton leaving the wirechambers and entering the ckov to get a ckov signal? I think that the beats at lower speeds are instrumental features.

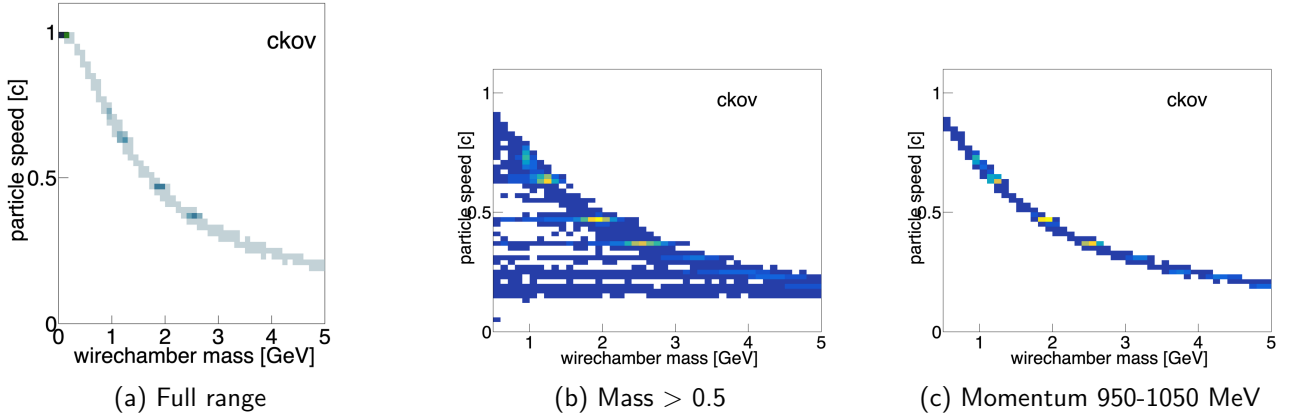


Figure 34: Speed against wirechamber mass. The left shows the full range, and is completely dominated by signals with  $\beta \sim 1$  and very low wirechamber mass. Center: Removing signals with wirechamber mass less than 0.5 GeV reveals peaks at higher masses, lower speeds. These peaks look suspiciously periodic. Right: Cutting tight on momentum to remove some of the noise, the peaks are clearly visible. **Look into this suspicion about instrumentation a bit more**

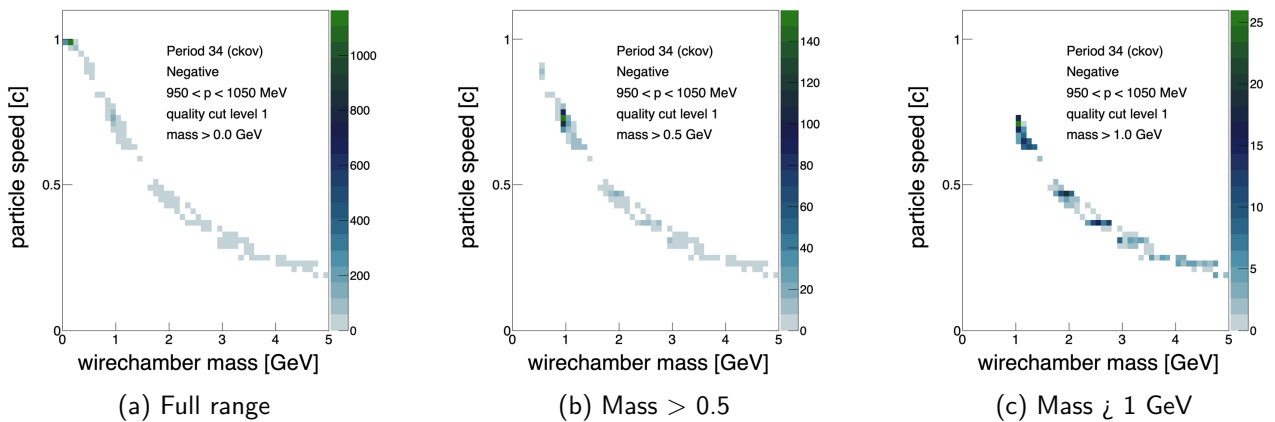


Figure 35: Nicer blots

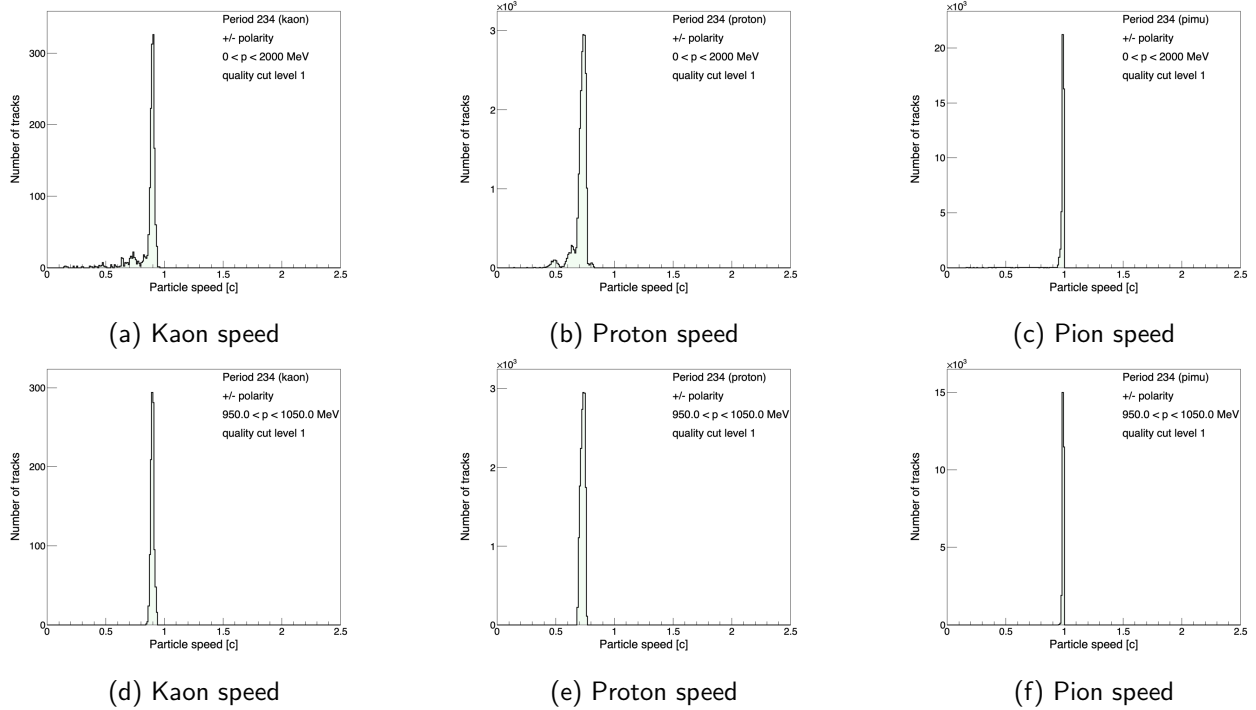


Figure 36: Speed of kaons, protons, pions. Top row is without a momentum cut, bottom row is with a momentum cut consistent with the current cuts.

## 7 Detector

The data in these plots is the full period4 dataset unless otherwise indicated, using the files in the definition `dduenas.pid.testbeam.beamlinestream.period4.magpol.bug_fix`. Selection cuts are:

- Pass the beamline trigger
- No detector deadtime
- Have a time-of-flight measurement
- Have at least one in-time detector hit.

### 7.1 The baby NOvA coordinates

Figure 37 shows the detector rotation.

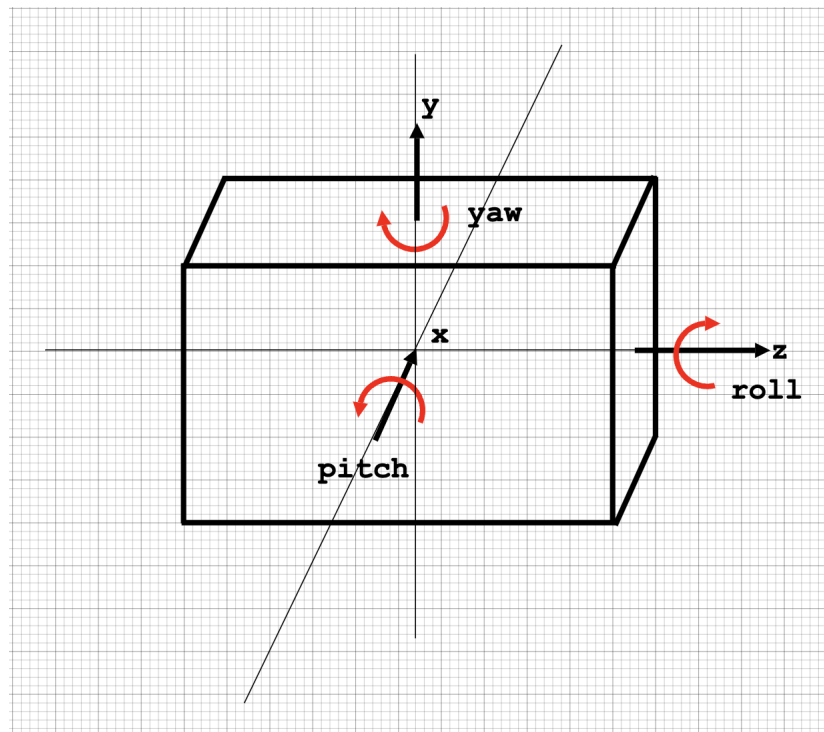


Figure 37: NOvA rotation.

### 7.2 Structure: Cells and Planes

There are 63 planes in the detector, each with 64 cells. The first plane, plane zero, has vertical cells. All the subsequent even-numbered planes have vertical cells, and the odd-numbered planes have horizontal cells. The basic geometry is as follows:

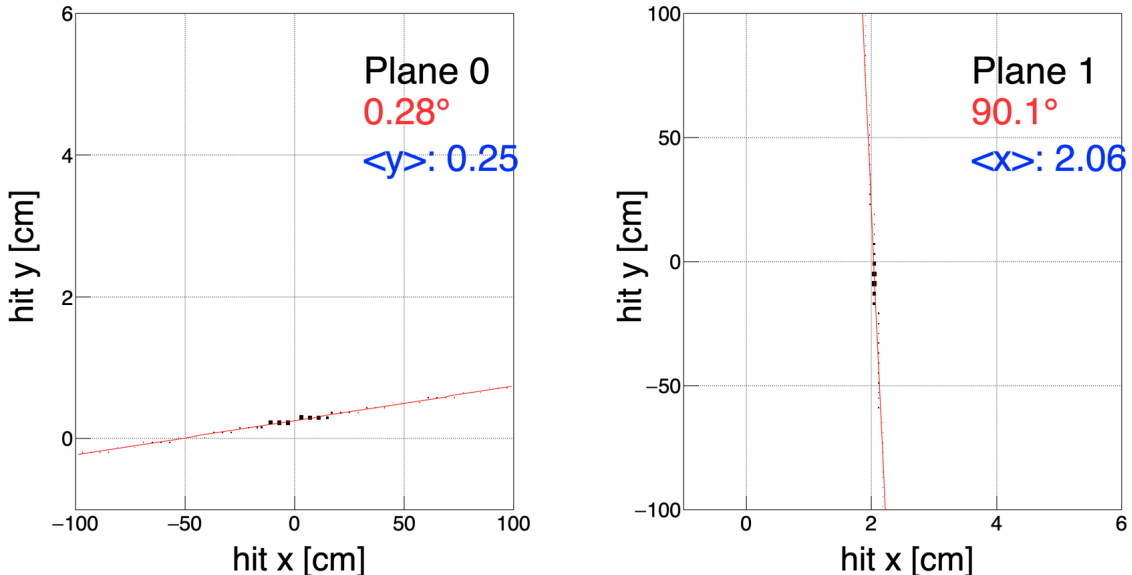


Figure 38: The xy positions of hits in (left) plane 0 and (right) plane 1. Plots made using the script `single-plot-detxy.py`.

The x-dimension runs east-west, from the center of cell zero at -124.706 cm to the center of cell 63 at +124.704 cm.

The y-dimension runs down-up, from the center of cell zero at -123.334 cm to the center of cell 63 at 126.078 cm.

The transverse half-width of the cells is 1.728 cm. For horizontal cells the transverse width is in y, for vertical cells it is in x.

The transverse half length of the cells is 130.820 cm. For horizontal cells the transverse width is in x, for vertical cells it is in y.

The z-dimension runs from the center of plane 0 at +3.383 cm to plane 62 at 418.033 cm. The half-depth of the cells is 2.782 cm.

The binning for the plots in this section uses the geometry considerations above, but the numbers above do not take into account the small shifts and rotations of planes with respect to one another.

Each plane is slightly rotated around the z-axis with respect to the superblock. This is just a fact of life, not something that was done deliberately. The rotations can be seen in Figure 38 for the first two planes, with the remaining plots available in Appendix 8 . A straight line fit provides the slope  $m$  and the angle is  $\theta = \arctan(m)$ . The angles have been checked against those in the testbeam survey [the testbeam survey](#) and are in agreement. Figure 39 shows the transverse position of cell hits as a function of z.

The energy deposited in calorimeter cells is recorded as PE (PhotoElectrons) and the calibration then converts this into a proper energy measurement in GeV. Figure 40 shows the before and after of this process for hits in plane 0 of the detector. The cells in plane 0 (and all subsequent even-numbered planes) are vertical, such that only a measurement of the x-position of a cell can be known. Figure 41 shows hits in plane 1 of the detector. The calibration fails in plane 1 (and all subsequent odd-numbered planes) because the horizontal cells were under-filled with scintillator early on in data taking, and this made it into the simulation. [Watch this space for updated plots with Robert's new calibration](#). These plots are available for every plane in Appendix 9. Figure 42 shows energy deposited as a function of z for uncalibrated and calibrated cell hit energies.

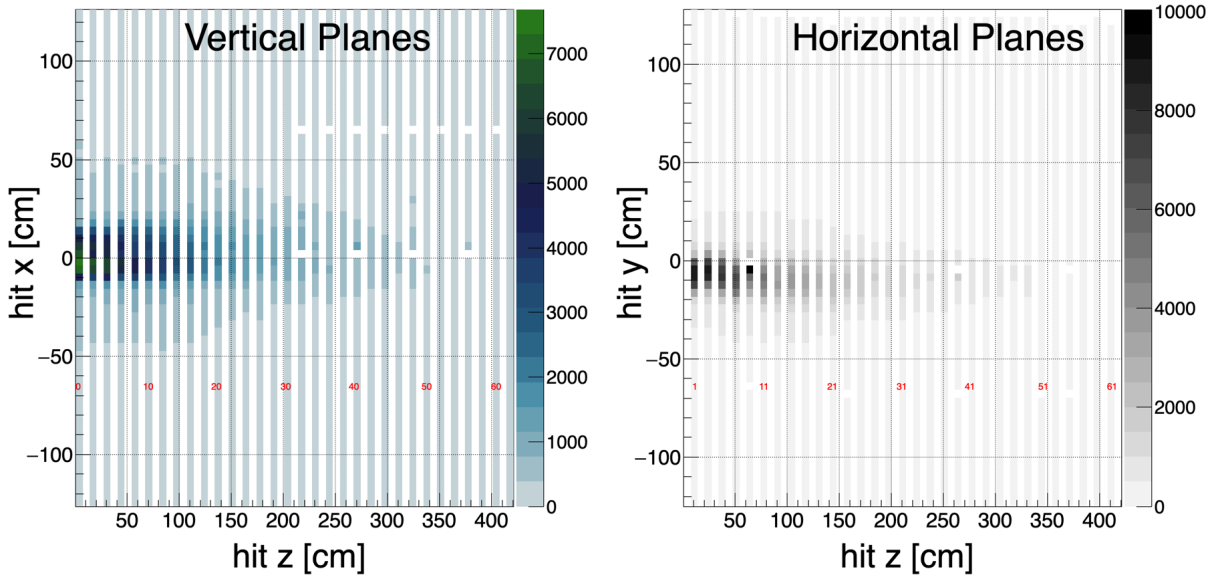


Figure 39: Detector cell hit  $z,x$  (left) and  $z,y$  (right) positions. There are a few empty bins which is just a result of the imperfect binning described in the text. Scripts are `single-plot-detxzdetail.py` and `single-plot-detyzdetail.py`

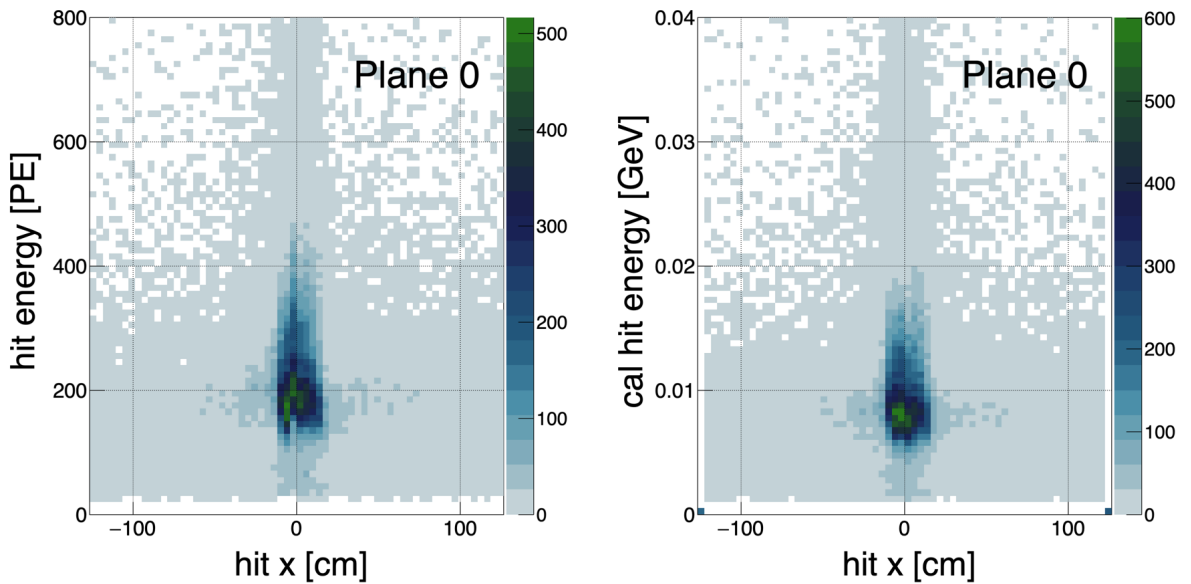


Figure 40: Plane 0 hit energies as a function of the cell positions within the detector for (left) uncalibrated hits and (right) calibrated hits. Scripts are `single-plot-detxpe.py` and `single-plot-detxgev.py`.

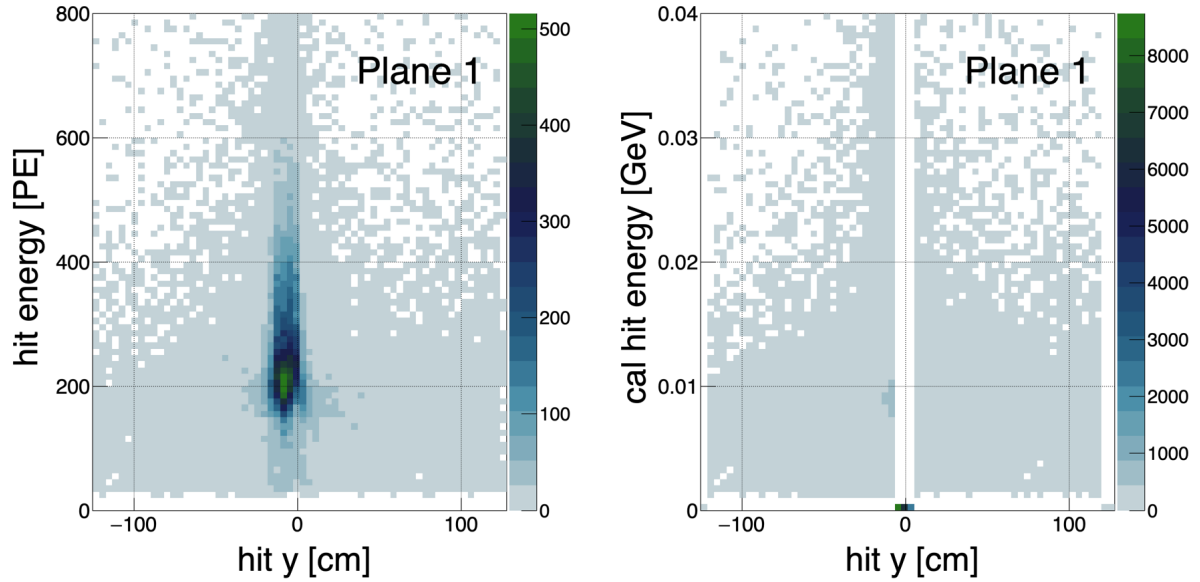


Figure 41: Plane 1 hit energies as a function of the cell positions within the detector for (left) uncalibrated hits and (right) calibrated hits.

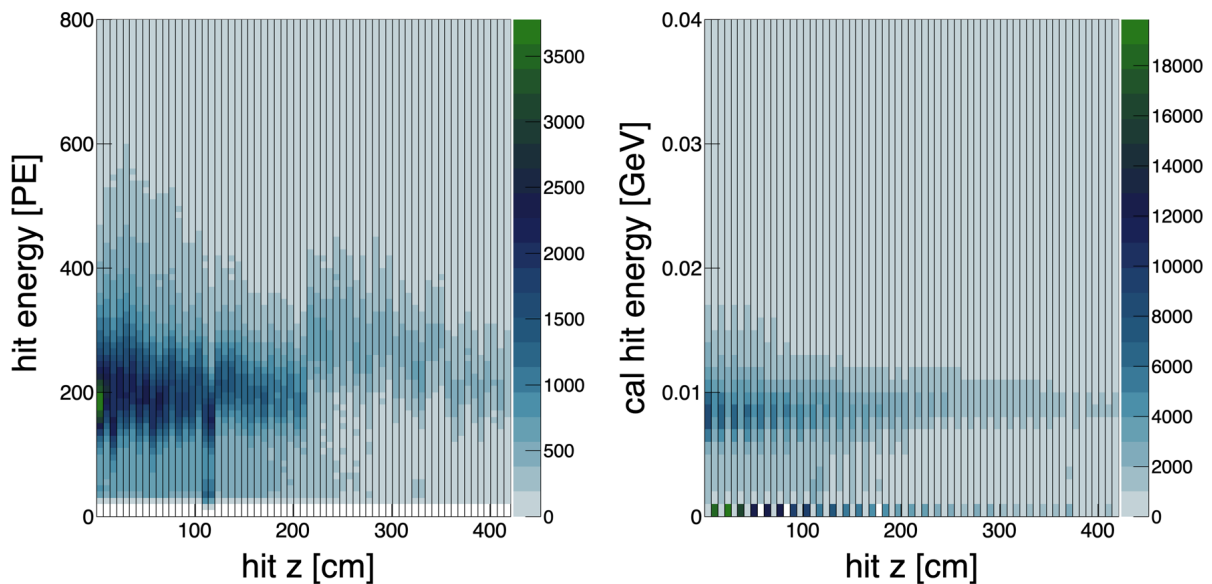


Figure 42: Detector cell hit energy (left) before and (right) after calibration.

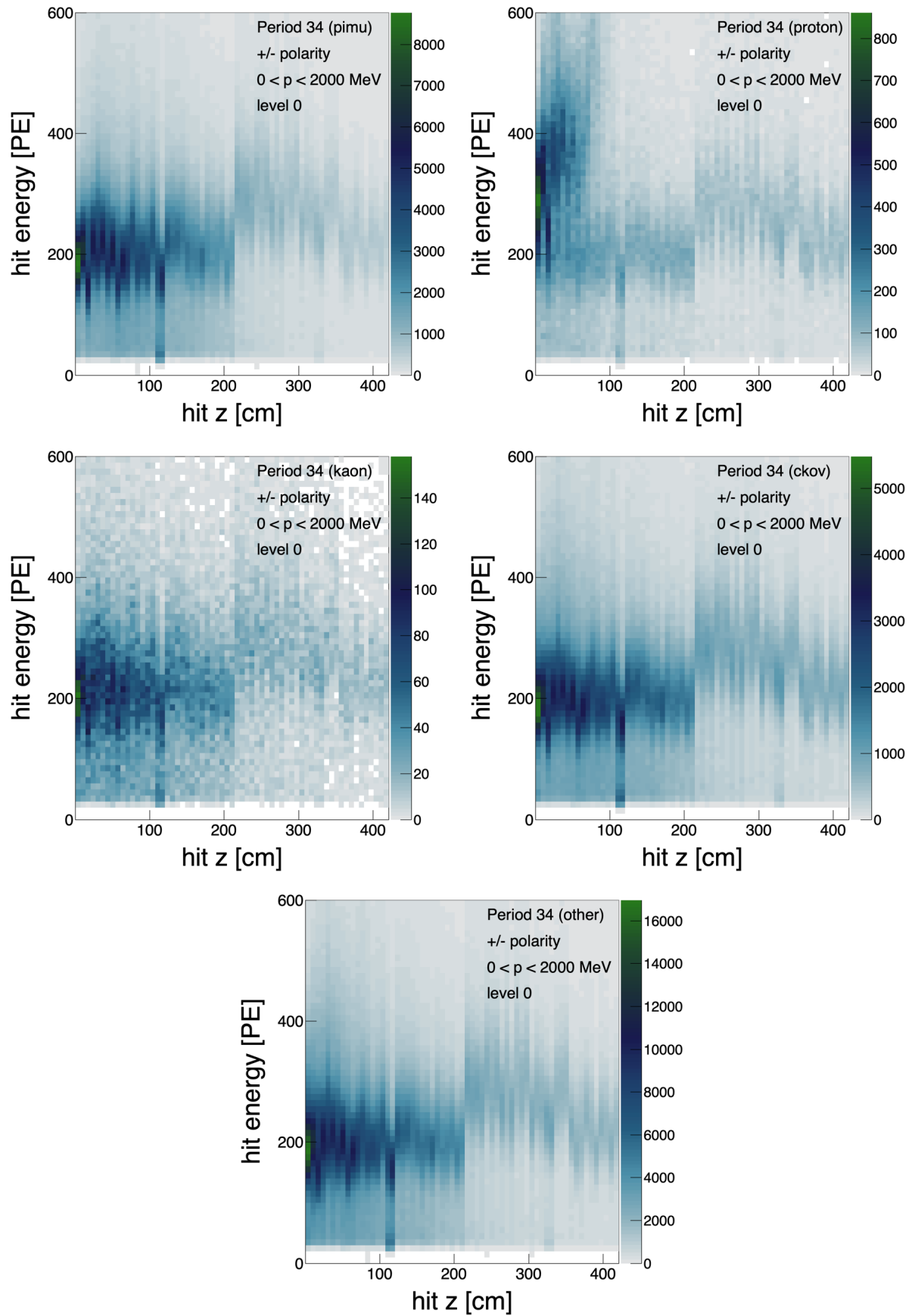


Figure 43: Hit Pe versus average  $z$  for different particles - script 2d-plot-style.py.

### **7.3 Hit properties**

Cell hits that are in time with the trigger can be matched to a beamline track (with “known” particle type). Here are some plots of some hit properties.

#### **7.4 Kinetic energy versus last plane with hit**

### **8 All the plots: detector plane rotations**

### **9 All the plots: Energy versus x/y**

Detector hit PE as a function of  $x(y)$  in vertical (horizontal) planes are show in Figures 53 and 54. Plots made using the script `single-plot-detxpe.py`.

Detector hit GeV as a function of  $x(y)$  in vertical (horizontal) planes are show in Figures 55 and 56. Plots made using the script `single-plot-detxgev.py`.

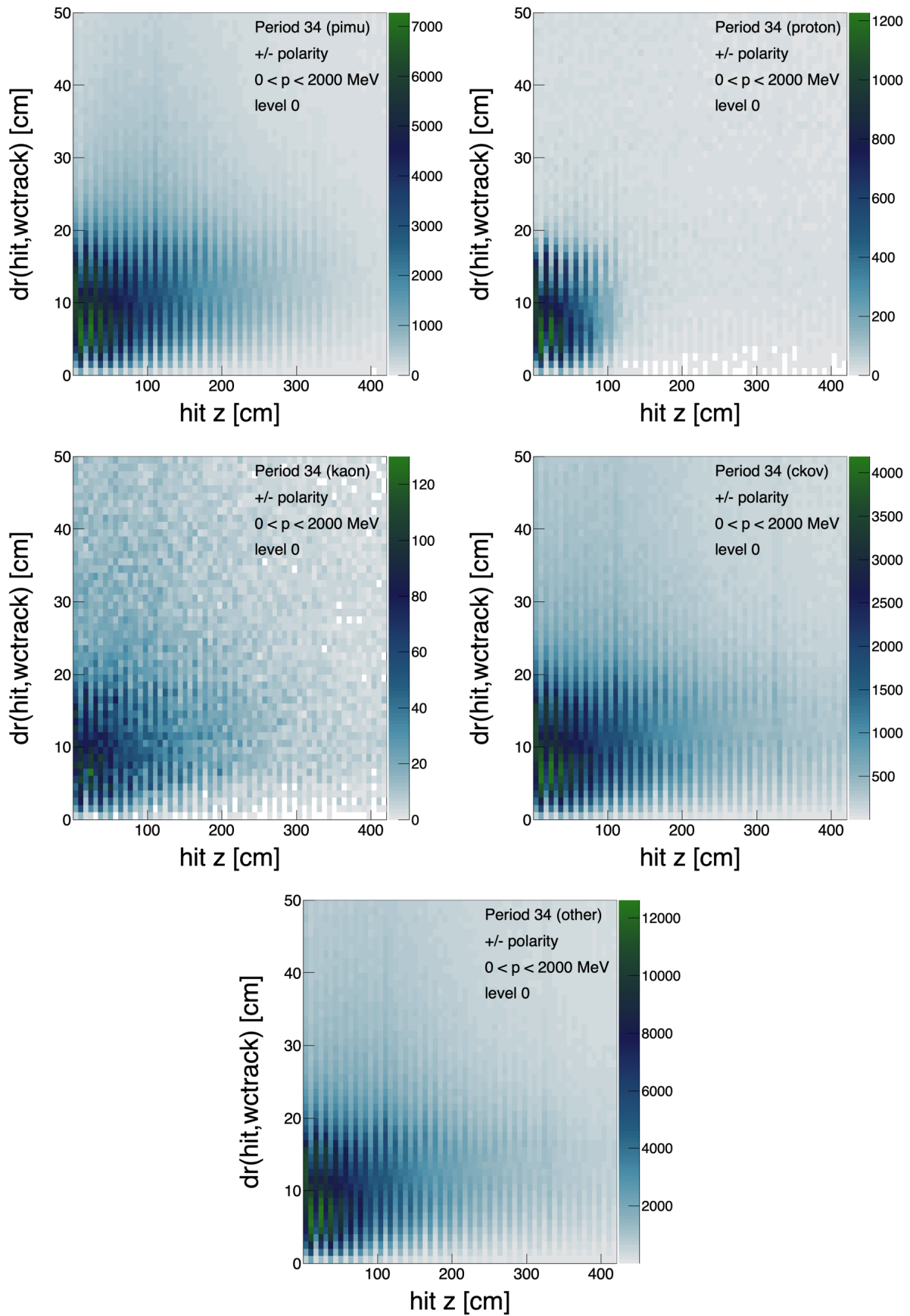


Figure 44: Drs - script single-plot-detdrzdetail.py.

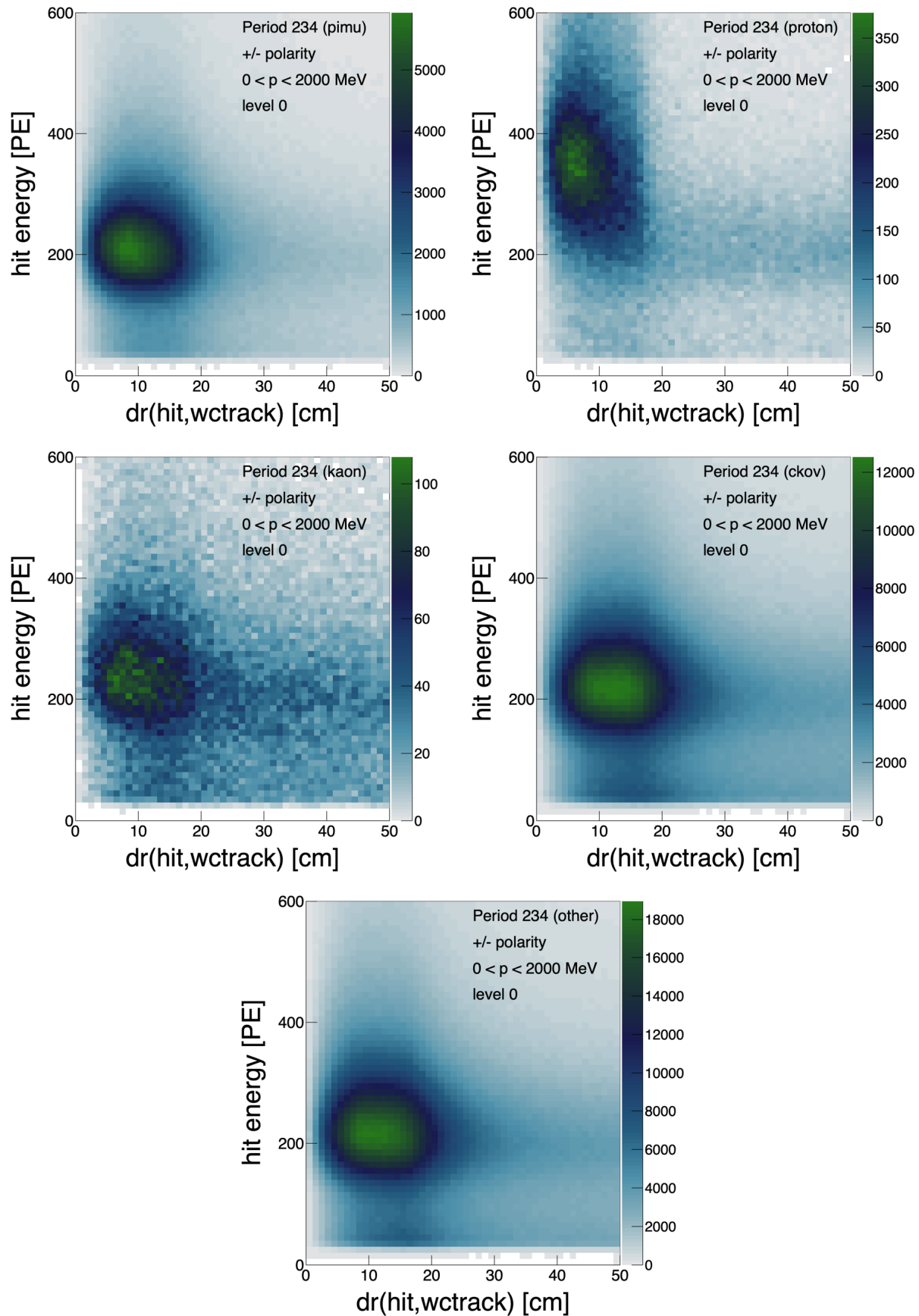


Figure 45: Dr versus PE - script 2d-plot-style.py.

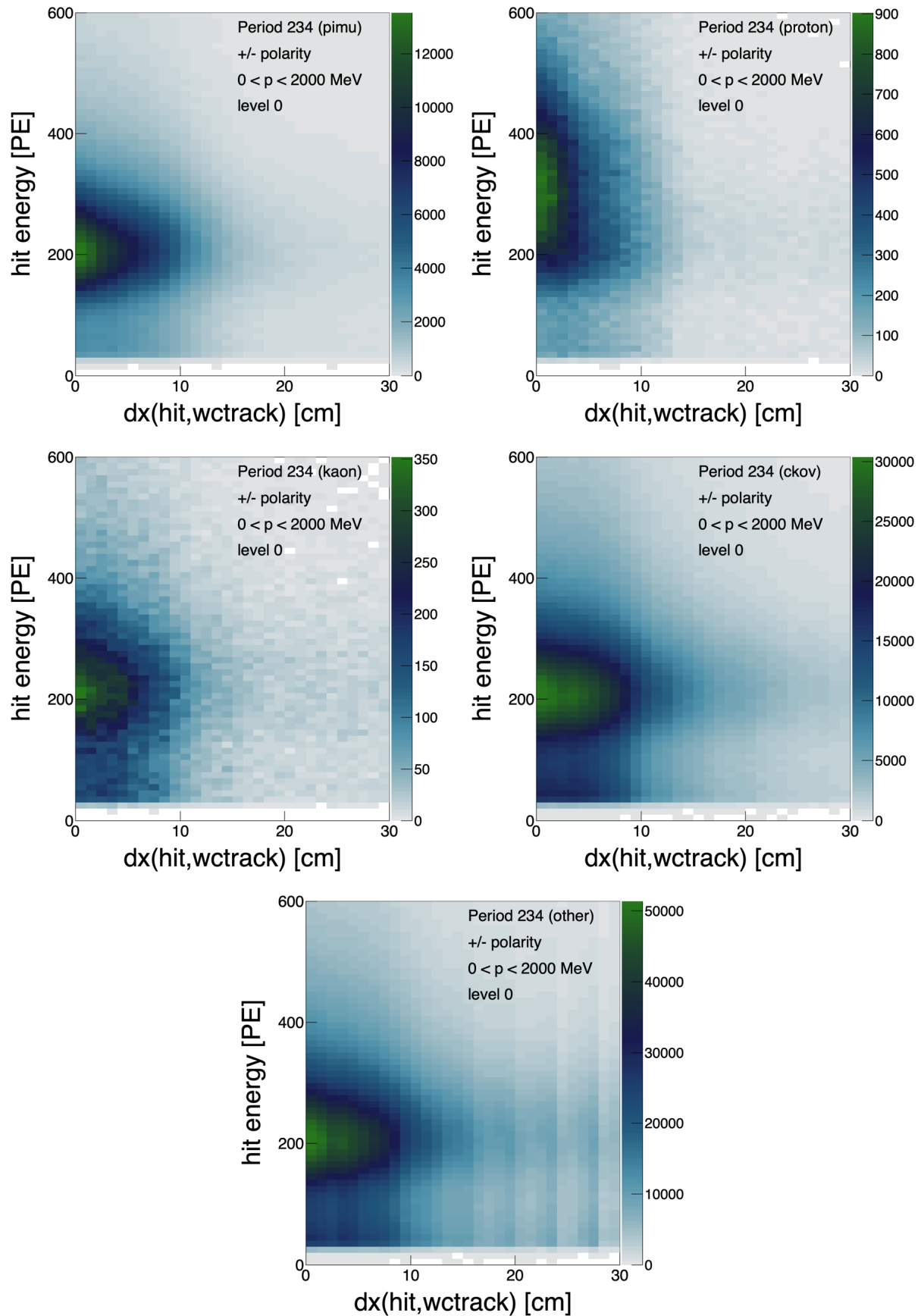


Figure 46: Dx versus PE - script 2d-plot-style.py.

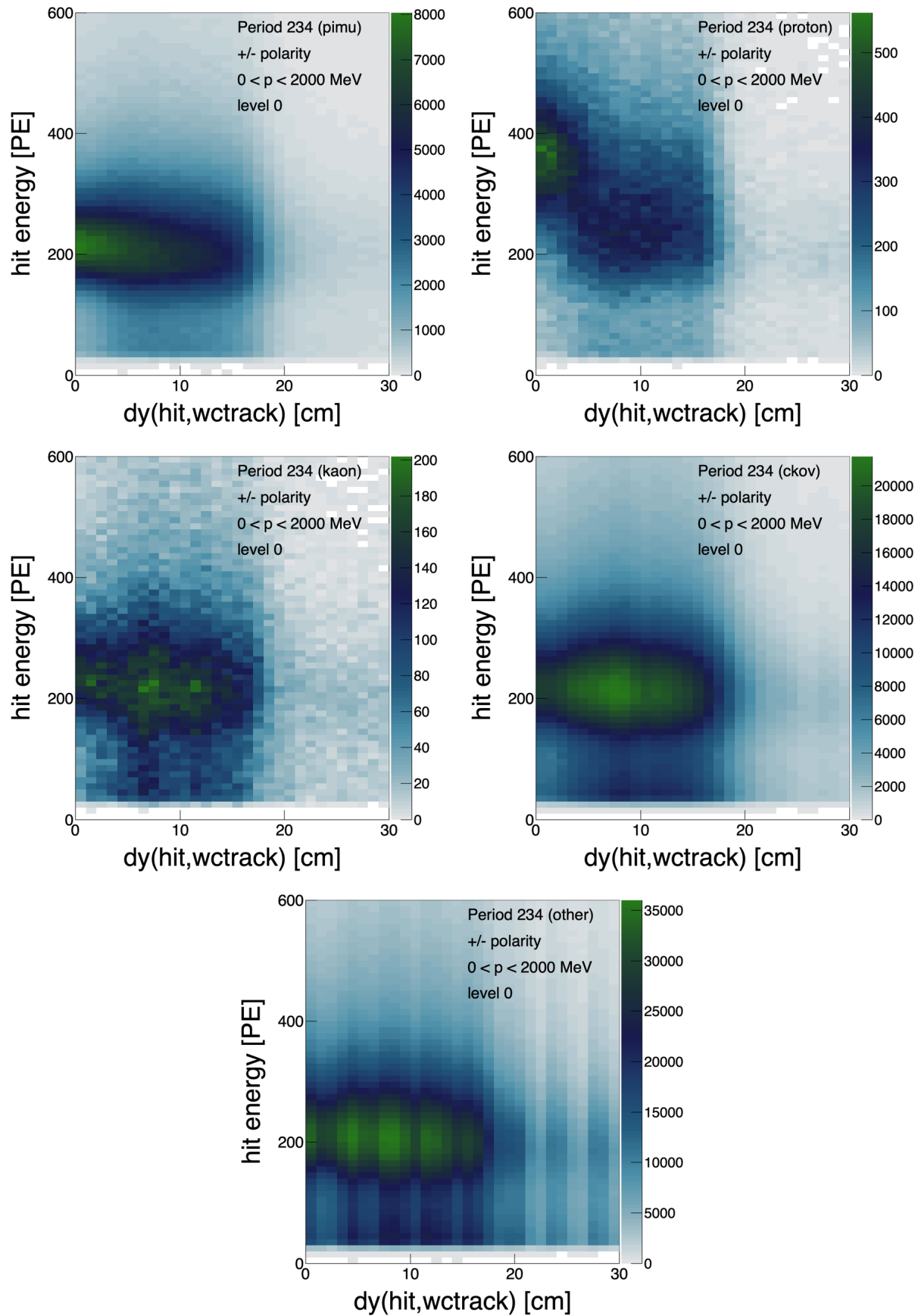


Figure 47: Dy versus PE - script 2d-plot-style.py.

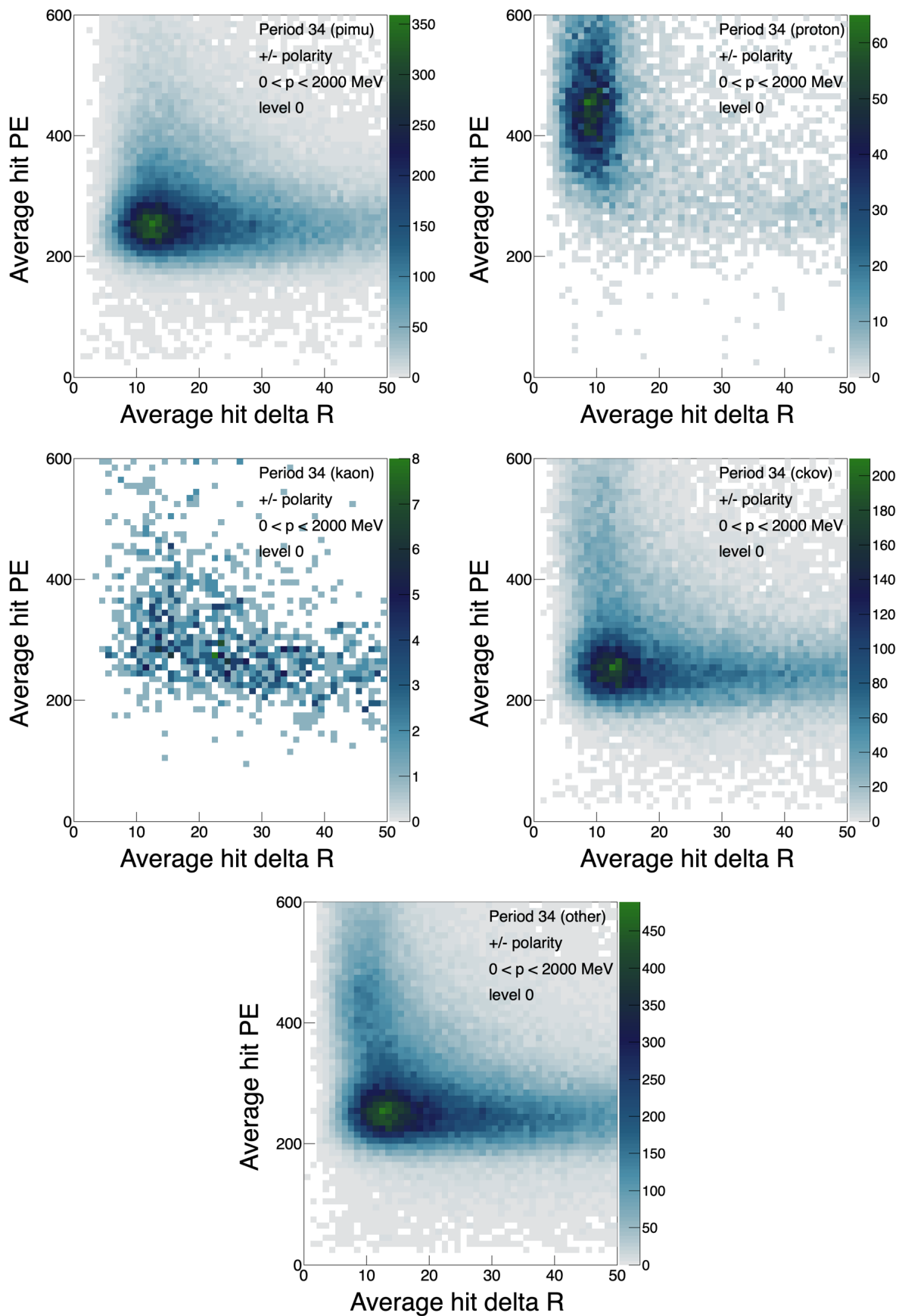


Figure 48: Average Dr versus average PE - script 2d-plot-style.py.

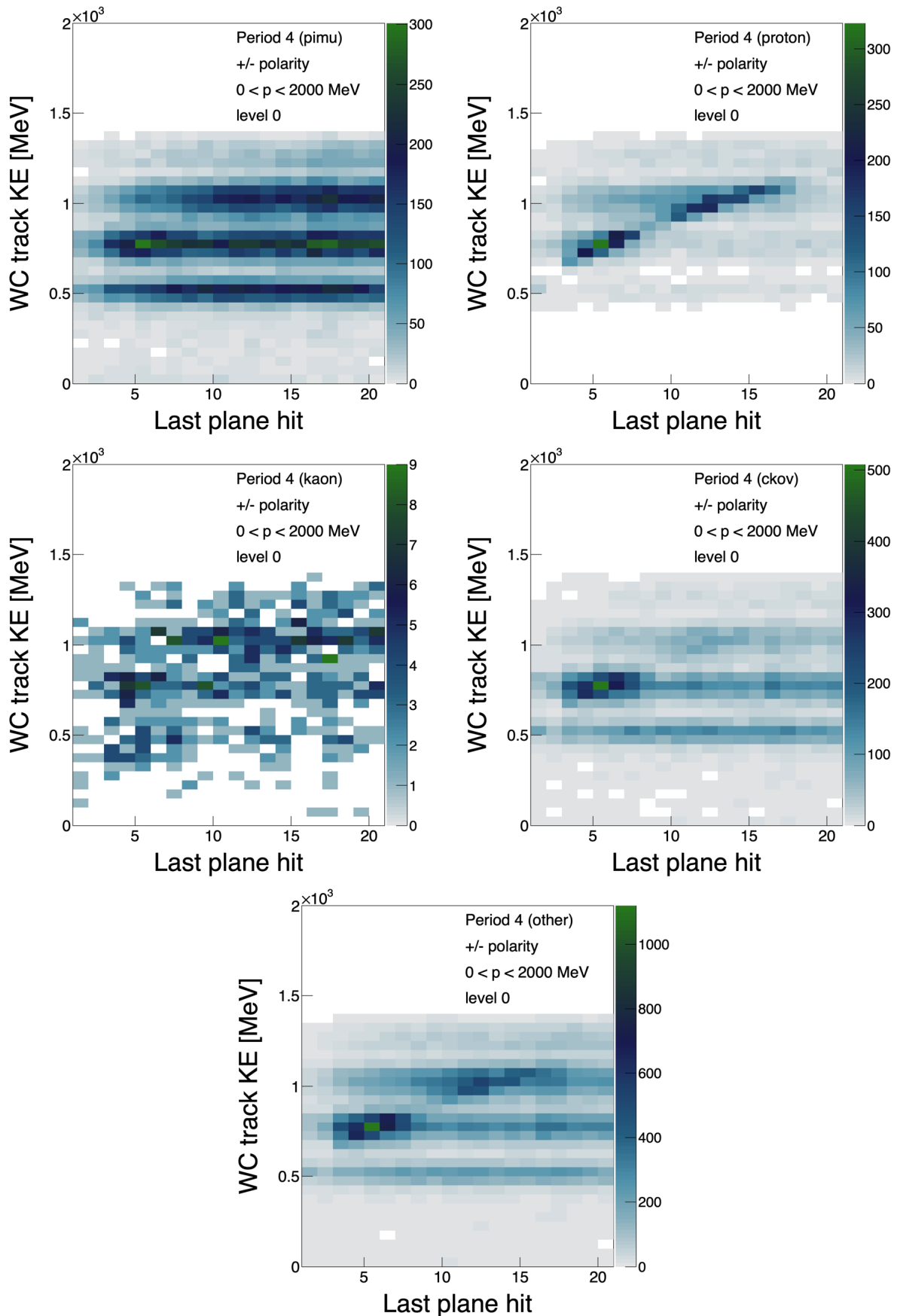


Figure 49: WC track KE versus last plane containing a hit (limited to planes 1-21) - script 2d-plot-style.py.

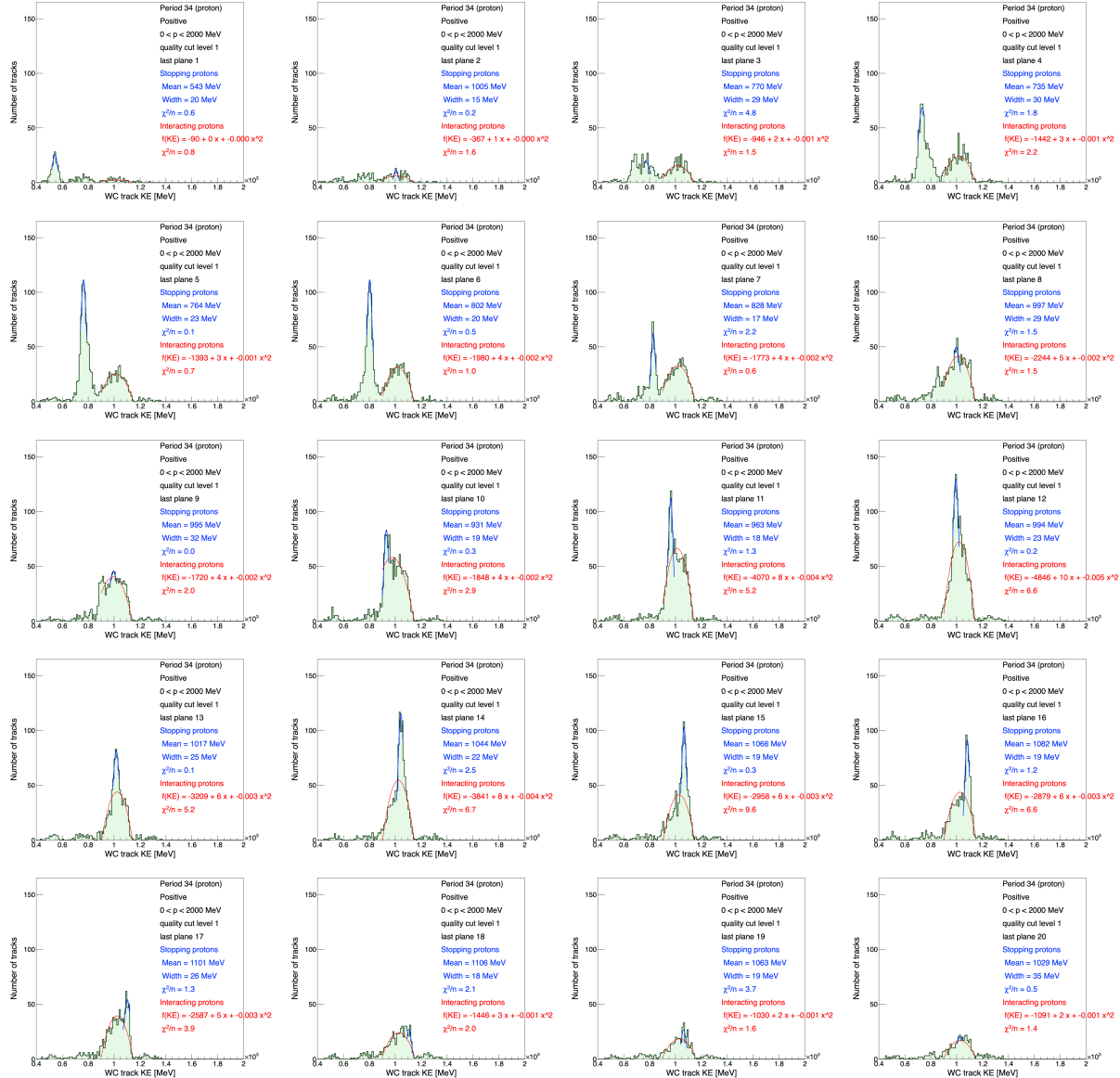


Figure 50: Kinetic energy of protons by plane of last hit- script 2d-plot-style.py.

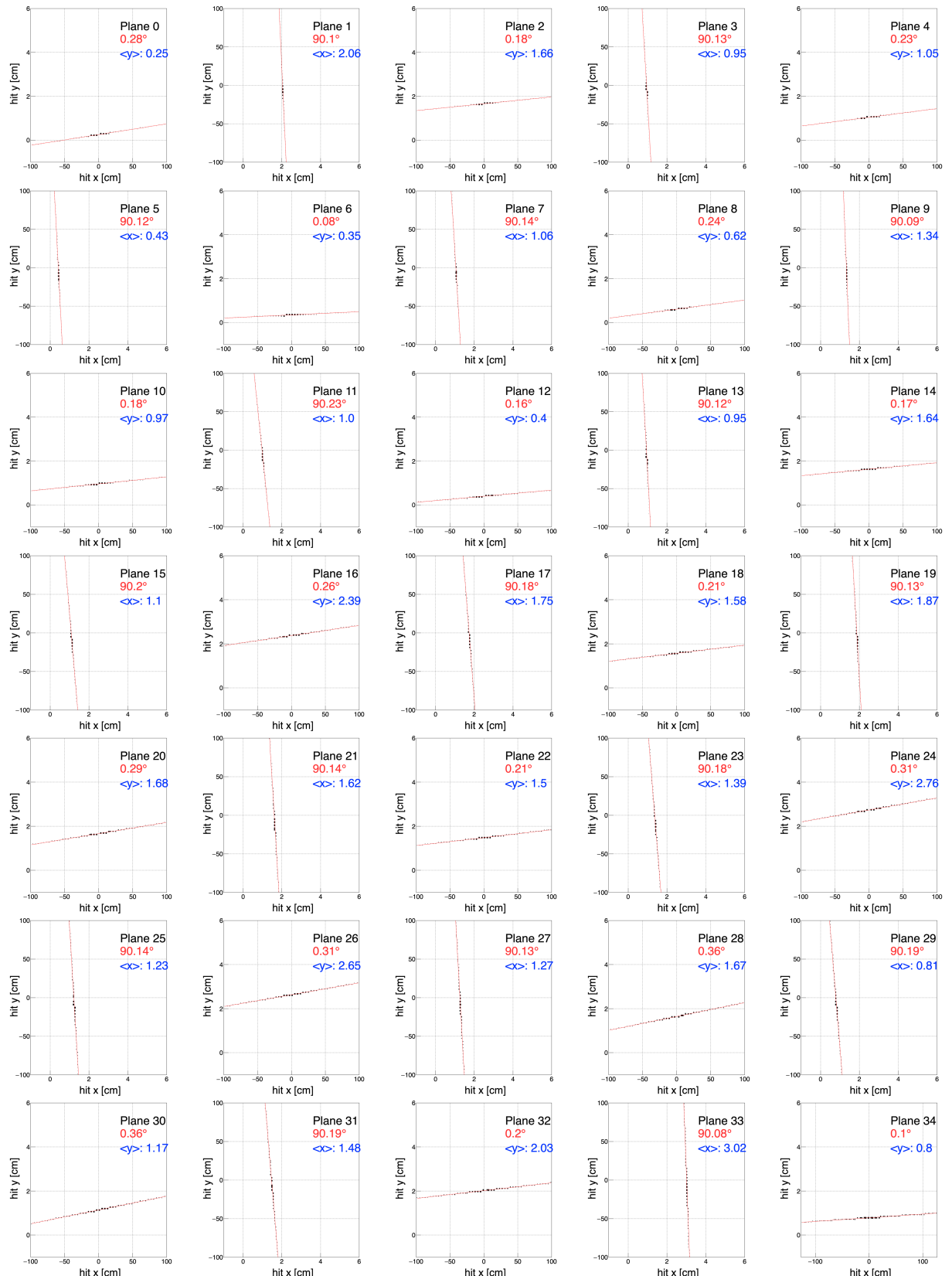


Figure 51: Detector hit positions by plane for the first 35 planes.

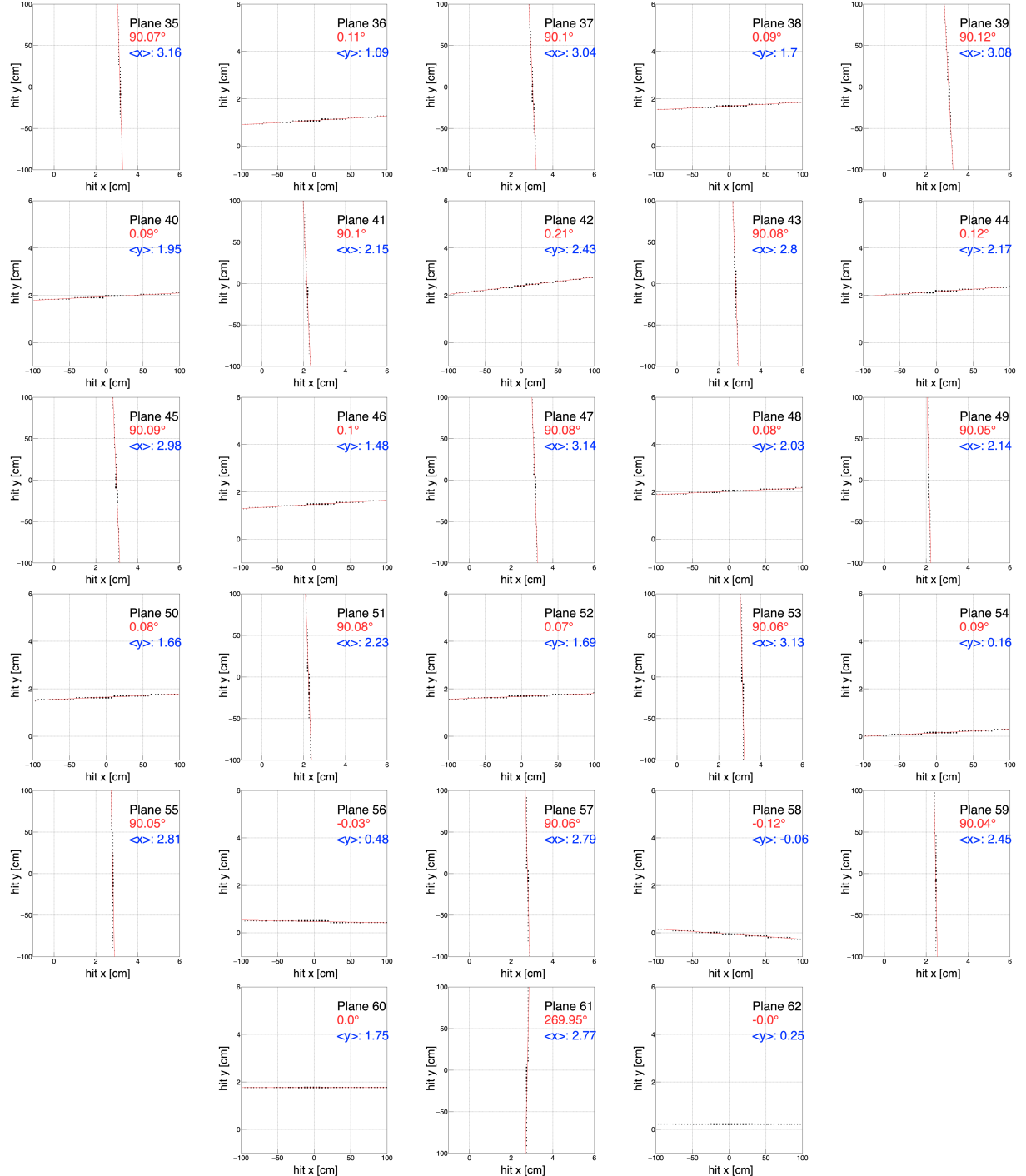


Figure 52: Detector hit positions in planes 35-62

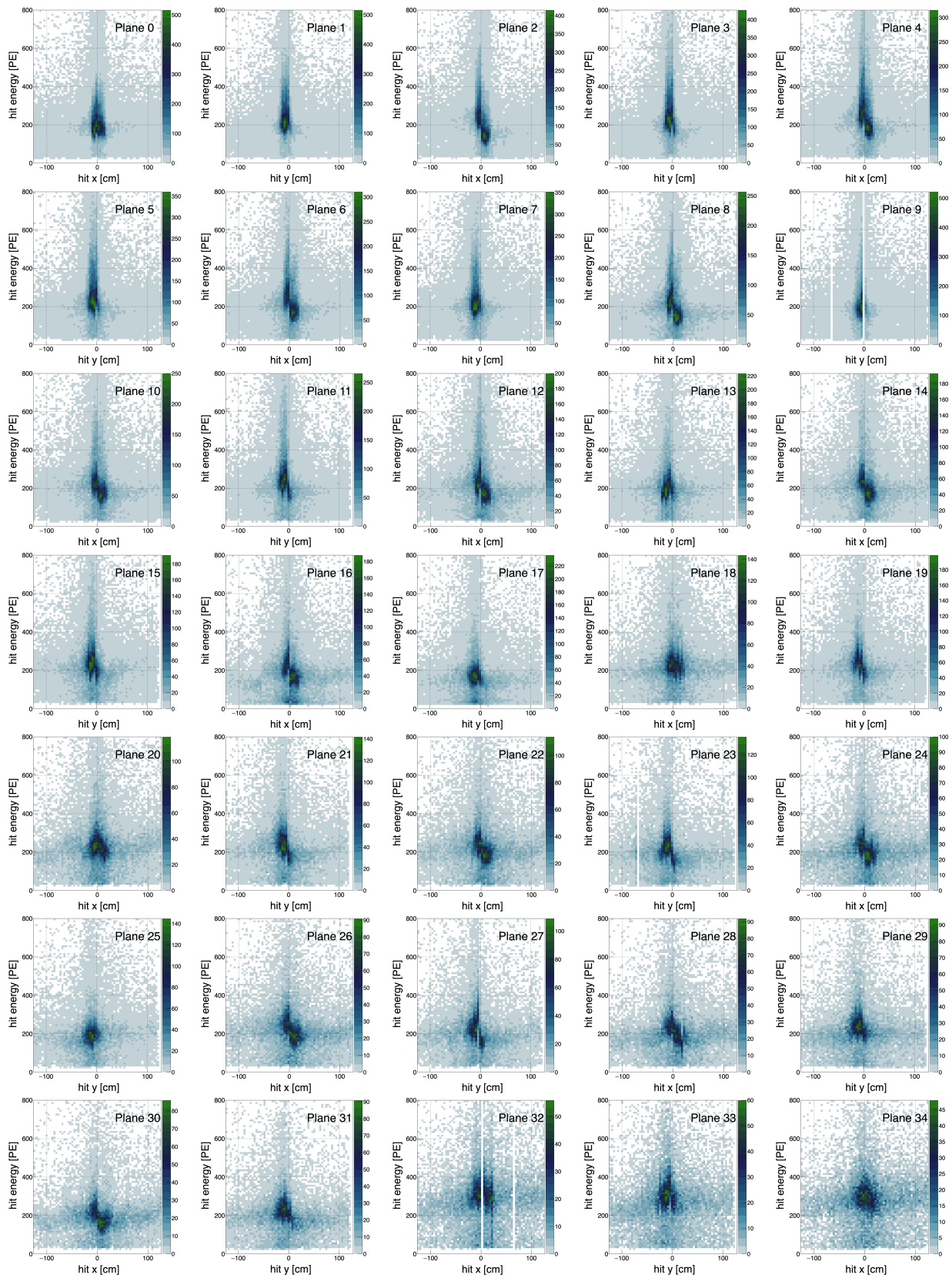


Figure 53: Detector CellHit PE by plane for the first 35 planes.

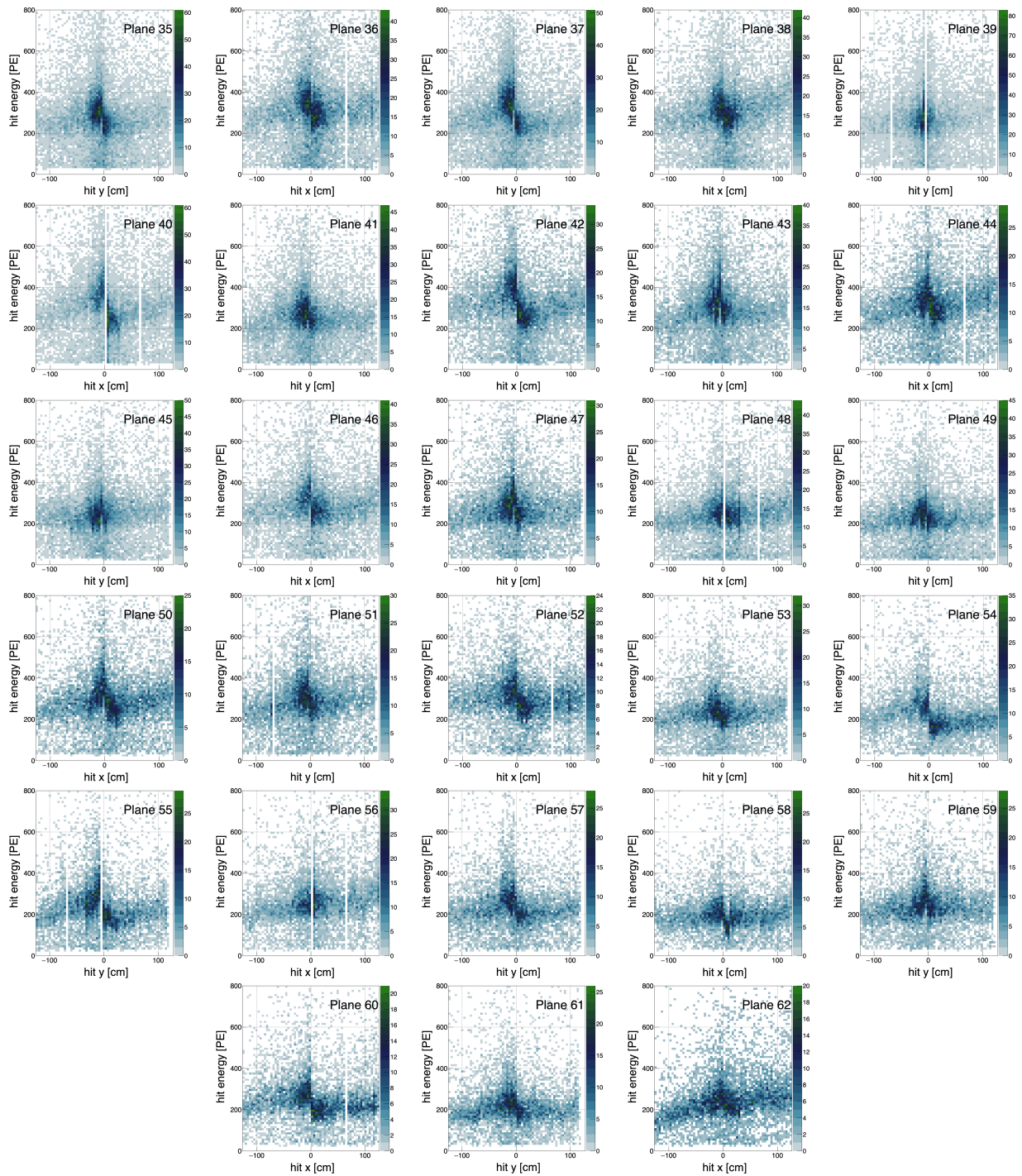


Figure 54: Detector CellHit PE in planes 35-62

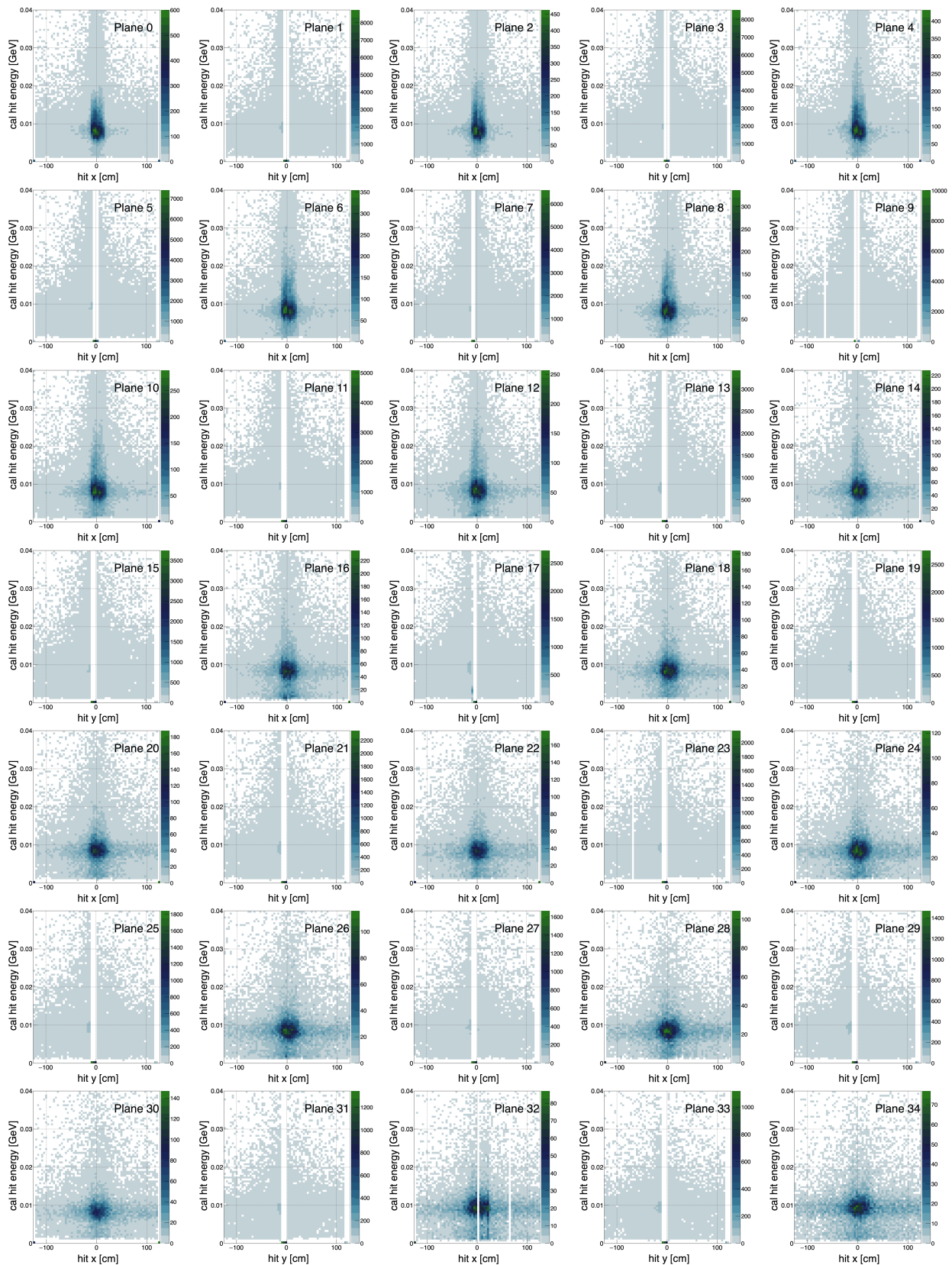


Figure 55: Detector CellHit calibrated energy aka GeV in the first 35 planes.

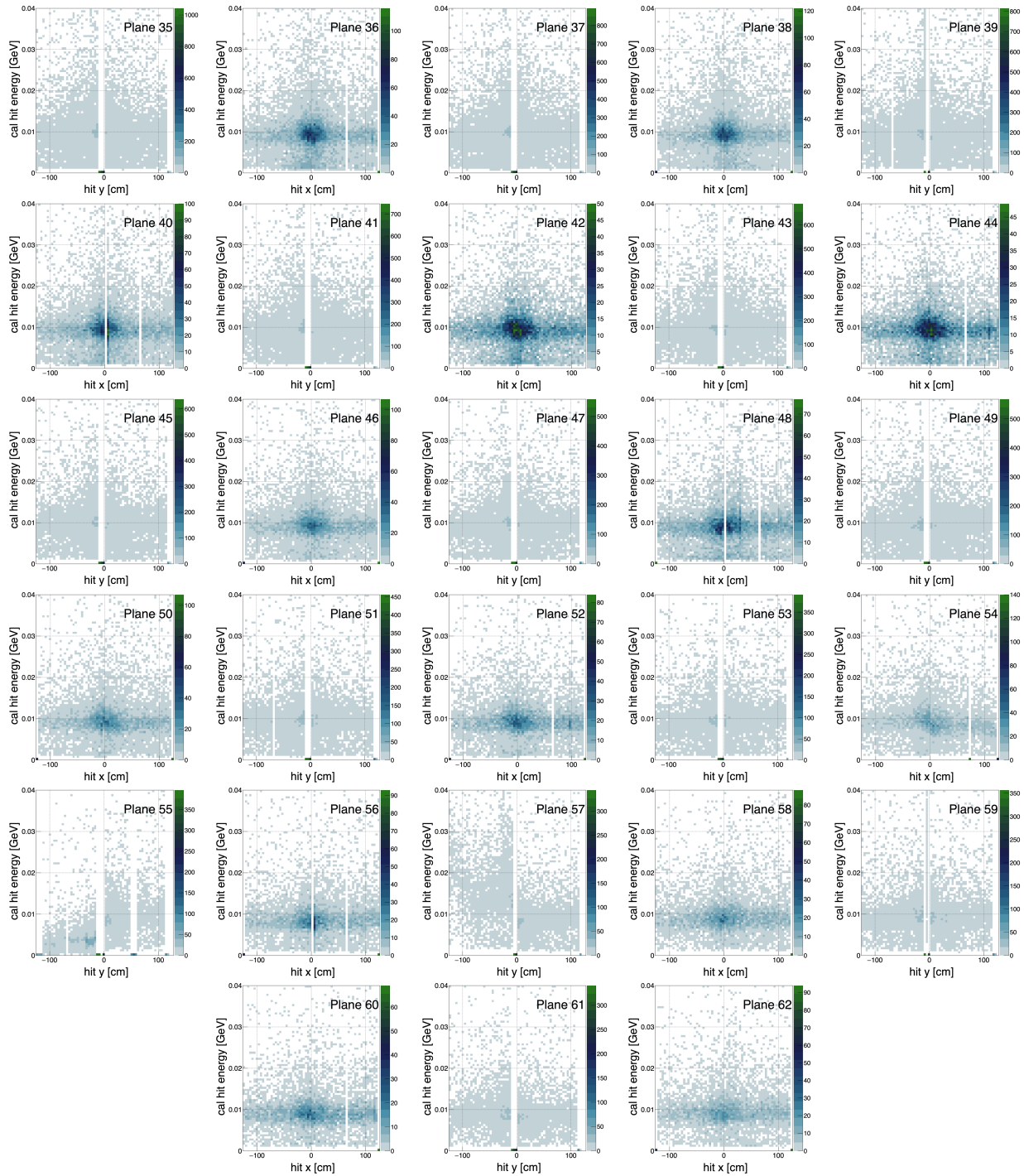


Figure 56: Detector CellHit calibrated energy aka GeV in planes 35-62